ACS OMEGA

Open Access

http://pubs.acs.org/journal/acsodf

Article

CH_4/NH_3 Flame Structure and Extinction Limit under Flame−Flame Interactions

Fanxing Meng, Quanwang Chen, Bingbing Zheng, and Xiaohan Ren*

Cite This: *ACS Omega* 2024, 9, 14997−15014

Read Online

ACCESS | Metrics & More | Article Recommendations

ABSTRACT: Ammonia is considered to play an important role in replacing traditional fossil fuels in future energy systems. In the experimental study, CH_4/NH_3 flame was lit by applying a double-nozzle burner to gain insight into the structure, and the laminar diffusion flame structure, CH*/OH* intensity maximum, and flame size were analyzed by an ICCD camera. In addition, the extinction limit (lower limit) of the CH_4/NH_3 flame under different conditions was also studied. The results showed that with the increase of burner pitch, the two diffusion flames showed four states of merged flames, merging flames, inclining separated flames, and independent flames in turn. In the process of flame separation, the continuous pitch between merging flames was short. At this point, higher syngas flow could help increase the continuous pitch to keep merging form. The paper investigated the flame structure and found that the flame size would decrease when the NH_3 content in the fuel was high. The flame stability also decreased with an increase of the NH_3 content in the fuel. These findings provided experimental proof and a theoretical basis for future studies on the stability of CH_4/NH_3 co-firing.

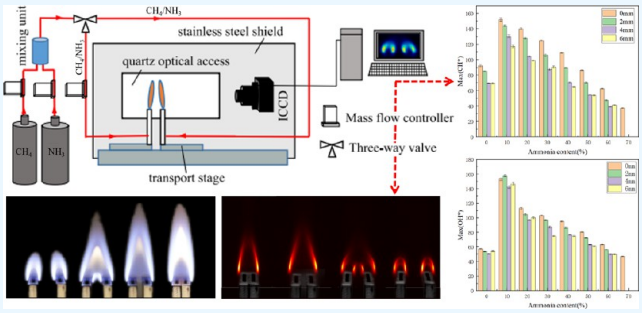

1. INTRODUCTION

The reduction of CO_2 emissions has become a common challenge for all mankind due to the increasing global warming caused by the large amounts of emissions from coal fuel combustion.[1] Methane (CH_4) has potential as a clean fuel to replace current heavy hydrocarbon fuels.[2] However, global warming due to carbon dioxide (CO_2) emissions continues despite the increasing use of cleaner fuels. As a result, the energy industry structure, which is overly dependent on fossil fuels (including CH_4), will inevitably shift to be partially replaced by low-carbon energy sources, including renewable energy. Hydrogen has long been considered one of the most promising renewable and clean fuels. However, the storage and transportation of hydrogen have been the technical bottleneck that restricts the utilization of hydrogen as a fuel for combustion.[3] Ammonia (NH_3), as a carbon-free, renewable alternative fuel, has the advantages of low cost, high volumetric energy density, easy liquefaction, storage, and transportation compared to hydrogen.[4,5] In addition, the current large-scale ammonia production is very stable.[6] And ammonia can be liquefied more easily than pure hydrogen, significantly reducing transportation costs and its associated development costs.[7] As a result, more and more researchers are looking at using ammonia as a fuel to replace carbonaceous fuels such as coal.[8−11] However, the application of ammonia combustion is also greatly hindered by difficulties including, among others, ammonia's relatively low laminar flame speed,[12] low adiabatic flame temperature,[13] high minimum ignition energy,[9] narrow flammability limits,[14] and high nitrogen oxide (NO_x) emissions.[9,12,13,15]

The technical strategy of ammonia blending with active fuels is used to solve the mentioned challenges of ammonia combustion. Due to the continued increase in global natural gas production,[16] CH_4/NH_3 fuels are considered the actual alternative fuel to NH_3/H_2 fuels. Compared to pure CH_4 combustion, CH_4/NH_3 co-combustion improves the low reactivity of pure NH_3 and reduces CO_2 emissions, but does not involve storage and transportation issues or safety concerns. The use of CH_4-NH_3 blends has recently been suggested as a low-carbon fuel because CH_4 can compensate for the low ignition energy and combustion intensity of NH_3, while NH_3 can help reduce CO_2 emissions.[17,18] The blow-off limit of diffusion flames has been studied for a long time.[17] However, the stability range also has a lower limit, where extinction occurs due to heat loss at the burner edge. Since the jet velocity at the extinction limit (lower limit) is very small under real conditions,

Received: November 14, 2023
Revised: March 8, 2024
Accepted: March 13, 2024
Published: March 23, 2024

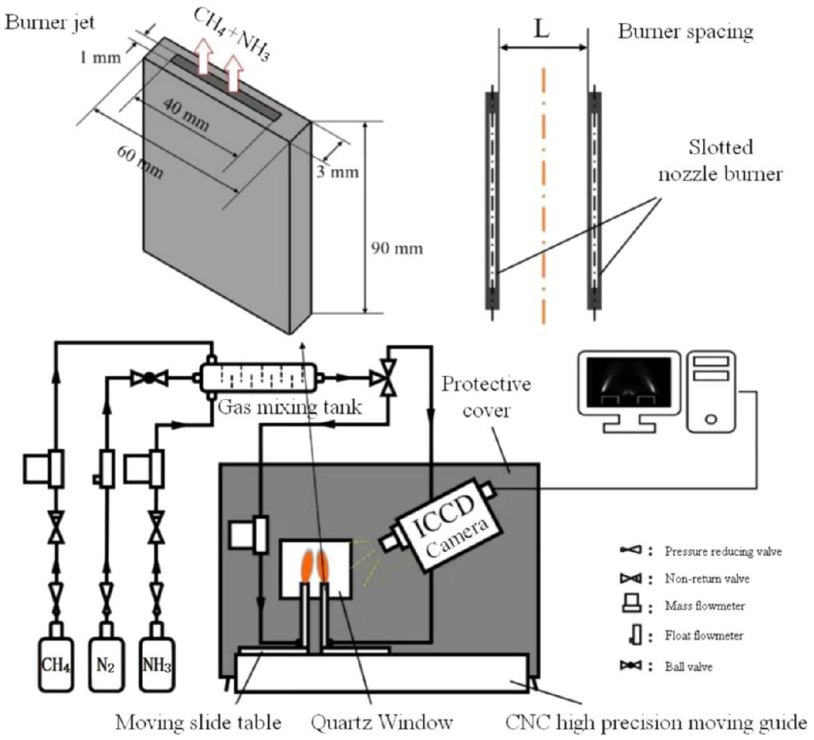

Figure 1. Schematic diagram of the laminar diffusion flame interaction test bench.

little attention was paid to this limit. Therefore, it is important to study the combustion characteristics of CH_4/NH_3 co-combustion and the extinction limit. Ramos et al.[19] and Shu et al.[20] found that the addition of methane to ammonia fuels almost linearly promoted the laminar combustion rate of NH_3/air flames. Colson et al. conducted an experimental study on the stabilization mechanism of CH_4/NH_3 non-premixed jet flames. It was found that the flame position shifted toward the jet and downstream when ammonia was added to the fuel compared to the methane non-premixed jet flame.[21] Skreiberg et al. studied the oxidation of ammonia under fuel-rich conditions in the presence of H_2, CO, and CH_4 below 1400 K.[22] Tian et al. studied a series of low-pressure premixed $NH_3/CH_4/O_2$/Ar flames to determine the effect of different CH_4/NH_3 molar ratios and proposed an NH_3/methane premixed combustion chemistry based on the Skreiberg mechanism. In this study, ammonia was added to the fuel mixture only as a minor component.[23] Ji et al. discussed the macroscopic structure and critical blow-off mechanism of NH_3/air flames near blow-off, and the effect of CH_4 addition on flame topology and flame stability. The results showed that the poor fuel quenching limit of NH_3/air flame is low and the NH_3/air mixture cannot be ignited when the fuel flow rate was greater than 5 m/s. With the addition of 50%CH_4 to the fuel, the laminar flame speed S_L and extinguishing strain rate K_{ext} were about 3 and 7 times higher than those of NH_3/air flame with Φ = 0.8 equiv ratio, respectively, and the flame was more stable.[24] Xiao et al. studied the properties of CH_4/NH_3 fuel stretching premixed flames at atmospheric pressure and ambient temperature and found that the addition of methane could help maintain a high flame stretching effect and therefore promoted the combustion stability of ammonia fuels.[25]

The validation of kinetic mechanisms was limited by the relative scarcity of Laminar burning velocity (S_L) data and the dispersion between different measurements. Mixtures of ammonia with hydrogen,[26−30] methane,[30,31] and syngas[32,33] have also been studied at atmospheric and high pressures. At the same time, data on laminar combustion velocities for flames with a high NH_3 content are still scarce.

Considering the above reasons, we therefore focused in this study on obtaining the laminar flame action of CH_4/NH_3 mixing firing under different experimental conditions in order to determine its reasonable combustion conditions.[34] And a dual-nozzle burner with adjustable pitch was applied to achieve the CH_4/NH_3 adjacent flame interaction. The specific goals were as follows: First, the CH_4/NH_3 diffusion flame morphology was studied. The instantaneous CH* and OH* concentration distributions were measured with an ICCD camera and averaged over 400 consecutive images to reduce the errors. The appearance of the flame morphology, CH*/OH* intensity maximum, and flame size were obtained under different conditions. Then, the fuel composition, fuel flow, and burner pitch were studied and discussed as the main factors. Second, the extinction limit of the CH_4/NH_3 diffusion flame was studied to provide a stable combustion range as various NH_3 ratios in the fuel mixture. The improvement of this paper over previous studies is the application of a multinozzle burner with a variety of experimental conditions to solve the above ammonia flame combustion problem. The fuel was not ejected independently of each other, and there was strong material diffusion and energy transfer between adjacent flames.[35] Interference between the airflow of each nozzle had a certain effect on the temperature, components, and velocity distribution of the reaction flow.[36] These changes in physical characteristics affect the heat and mass transfer process, followed by changes in residence time and reaction time, followed by changes in chemical reactions. The physical and chemical processes ultimately determined the flame combustion characteristics such as flame front position, combustion intensity, and stability.

https://doi.org/10.1021/acsomega.3c09073
ACS Omega 2024, 9, 14997−15014

2. EXPERIMENTAL METHODS

2.1. Diffusion Flame Interaction Combustion System.

2.1.1. Experimental Bench Air Distribution System. Based on the idea of simplifying a three-dimensional flame into a two-dimensional combustion, two slot burners were used in this experiment to experimentally measure the flame interaction, and the structures of the burners are shown in Figure 1. The CH_4, NH_3, and N_2 used in the experiments were supplied from high-pressure cylinders. CH_4 and NH_3 gases are routed through a pressure reducing valve and a check valve, subsequently passing through a mass flow meter to regulate their flow rates. Within the gas mixing tank, they are thoroughly blended through the pipeline before being supplied to the burner for combustion. A Beijing Seven Star digital mass flow meter was used for fuel flow control. CH_4 and NH_3 were controlled by a 2000 mL/min (corresponding to the volume flow rate at standard state 1 atm, 0 °C) flow meter and a 2000 mL/min flow meter, respectively, with an accuracy of ±1% of the specified point or ±0.35% of the full scale, and a response time of ≤1 s. Folded plates were added to the mixing tank to ensure the adequate mixing of CH_4 and NH_3. N_2 in the high-pressure cylinder, through the pressure-reducing valve, floats a flow meter into the mixing tank, used to exhaust the residual gas mixture in the tank and pipeline after the experiment.

2.1.2. Flame Interaction Combustion Device. Based on the idea that a multinozzle burner can better improve flame combustion, two slotted burners were used for experimental measurements of flame interaction in this experiment, and the burner structure is shown in Figure 2. The single nozzle outlet

Figure 2. Flame interaction burner physical picture.

section of the burner is 1 × 40 mm^2 and the inner cavity is 85 mm high to ensure uniformity of the gas outlet velocity with a mechanical machining accuracy of less than ±0.02 mm. Two burners of the same size are fixed on a high-precision moving guide, and the distance between the burners can be changed by adjusting the guide, which is controlled by a stepper motor with an adjustment accuracy of ±0.02 mm. In order to reduce the error in the flow rate at the outlet of the two burners caused by the different resistance along the pipe and at the burner interface, a mass flow meter of 2000 mL/min was installed between the mixing tank and one of the burners to ensure the same fuel flow rate in both directions.

In addition, a 400 mm × 800 mm × 500 mm stainless steel shield with a quartz glass window at 0° was installed outside the burner to reduce the influence of external airflow on the flame interaction and the influence of background light changes on the flame photography.

2.1.3. Flame Optical Measurement. CH autofluorescence signal (CH*) and OH autofluorescence signal (OH*) were studied by using an ICCD camera in variable pitch laminar diffusion flame. CH* is an excited radical, produced spatially close to the first sharp temperature increase in the flame reaction zone, resulting in a blue/violet photon profile commonly termed a "flame". CH* is mainly present within the flame front, distributed on the side of the oxygen-fuel contact surface close to the fuel, and is useful in identifying multiple flame parameters.[37] OH* is also mainly active near the flame surface and is often used to determine the location of flame fronts.[38] OH* is generally distributed on the side of the oxygen-fuel contact surface near the oxygen, while the concentration of OH* can be used to reflect the size of the heat release rate of combustion.[39] Therefore, both CH* and OH* were measured in this experiment to accurately reflect the structure of the inner and outer fronts of the diffusion flame. According to the measurement requirements, a CCD camera model SX 6 M from LaVision was selected together with an IRO X 55 ns image intensifier system with CH and OH filters for signal filtering. A digital signal delay generator (LaVision PTU X) was used to control the synchronization of the neodymium-doped yttrium aluminum garnet (Nd:YAG) laser and the ICCD camera, and Davis 10 software was used for data acquisition. The ICCD camera parameters were set as follows: exposure time 3801 μs, delay time 5 ns, gain 70%, and gate width 800,000 ns. The flame CH* and OH* distributions measured in this paper were averaged over 400 images taken in order to reduce the experimental error caused by excessive background noise and flame instability. The technical specifications of the imaging system are shown in Table 1, and the physical camera is shown in Figure 3.

Table 1. Imaging System CCD Camera Technical Indicators

designation	technical specifications	unit
pixel	2752 × 2200	pixels
pixel size	4.54 × 4.54	μm^2
exposure time	42−10^6	μs
spectral range	400−900	nm
frame rate	25	frame/s
minimum interframe time	150	ns
image recording format	12-bit grayscale value	none

Figure 3. ICCD camera physical diagram.

2.2. Working Condition Setting and Experimental Procedure.

In this paper, experiments are conducted to obtain the flame structure of methane-doped ammonia blending combustion under different conditions and the extinction limit of the flame by focusing on three conditions: fuel composition, fuel flow, and burner pitch.

https://doi.org/10.1021/acsomega.3c09073
ACS Omega 2024, 9, 14997−15014

Table 2. Experimental Conditions of CH_4/NH_3 Laminar Flame Interactions

fuel components	400 (mL/min) Re	500 (mL/min) Re	600 (mL/min) Re	700 (mL/min) Re	800 (mL/min) Re
100%CH_4	79.120	98.900	118.680	138.460	158.241
90%CH_4−10%NH_3	78.945	98.681	118.417	138.154	157.890
80%CH_4−20%NH_3	79.121	98.901	118.681	138.461	158.241
70%CH_4−30%NH_3	79.632	99.540	119.448	139.356	159.264
60%CH_4−40%NH_3	80.462	100.577	120.692	140.808	160.923
50%CH_4−50%NH_3	81.598	101.998	122.398	142.797	163.197
40%CH_4−60%NH_3	83.085	103.856	124.627	145.398	166.169
30%CH_4−70%NH_3	84.963	106.204	127.445	148.685	169.926

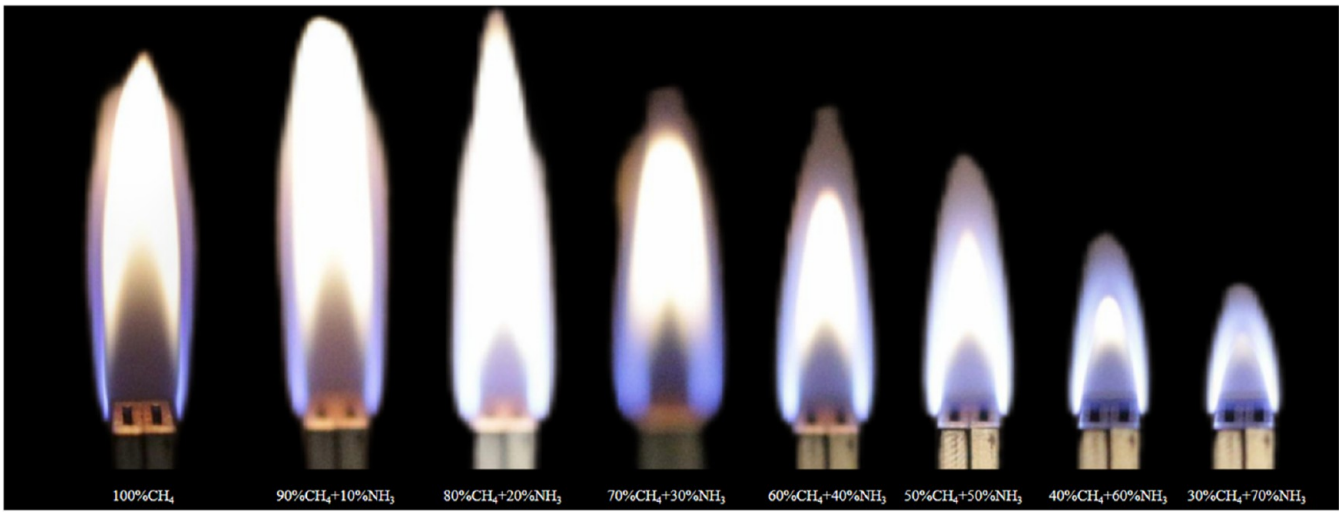

Figure 4. Pictures of flame appearance of different components of CH_4/NH_3 fuel at a fuel flow rate of 800 mL/min at 0 mm pitch (from left to right, the fuel composition is 100%CH_4, 90%CH_4−10%NH_3, 80%CH_4−20%NH_3, 70%CH_4−30%NH_3, 60%CH_4−40%NH_3, 50%CH_4−50%NH_3, 40%CH_4−60%NH_3, and 30%CH_4−70%NH_3).

2.2.1. Flame Structure. In order to obtain a clear flame structure and reduce the measurement error, the flame pulsation should be minimized, and the flame stability should be improved. In this experiment, according to the size of the burner and flame stability, the total fuel flow rate selected for the experimental conditions were 400, 500, 600, 700, and 800 mL/min, and the fuel blending ratios were 100%CH_4, 90%CH_4−10%NH_3, 80%CH_4−20%NH_3, 70%CH_4−30%NH_3, 60%CH_4−40%NH_3, 50%CH_4−50%NH_3, 40%CH_4−60%NH_3, and 30%CH_4−70%NH_3. Burner double-nozzle outlet total cross-sectional area $A = 8 \times 10^{-5}$ m^2. The average outlet flow rate is calculated by the equation $\upsilon = Q_v/A$. The velocity in the Reynolds number (Re) calculation is taken as the average outlet flow rate. The characteristic length is calculated by the formula $d = 4A/L$ for the rectangular equivalent diameter. The kinematic viscosity was obtained by using the "AP1700 online calculation and query platform for commonly used substances" under the ambient conditions of 25 °C and 1 atm. According to the calculation, all fuel flow rates are in the laminar flow range, as shown in Table 2.

2.2.2. Extinction Limit. The effects of fuel composition, fuel flow, and burner pitch on the interaction of CH_4/NH_3 flames were previously investigated. Next, in order to accurately describe the influence law of these factors on the extinction limit and to obtain reliable data on the extinction limit of CH_4/NH_3 flames under different conditions, it is necessary to conduct relevant experimental studies. The experimental part of this section covers:

(1) Variation of extinction limits with burner pitch for different fuel flow rates at 70−95% ammonia content in fuel composition.
(2) Variation of extinction limits with burner pitch for different fuel compositions at fuel flow rates of 400−1200 mL/min.
(3) Variation of extinction limits with fuel flow rate for different fuel compositions at burner pitch of 0−10 mm.

2.3. Experimental Data Processing.

(1) Maximum flame radius: First extract the maximum CH*/OH* intensity of each pixel row at the flame front in the flame CH*/OH* distribution diagram, then the center curve of the flame is derived by fitting the curve with polynomials. Finally, the maximum distance from the center curve to the symmetry axis of the two burners is extracted as the maximum flame radius, where the coefficient of determination of the fitted curve R is greater than 0.9.
(2) Flame length: The flame outline is difficult to determine due to the hairy flame edge and image background noise. In this paper, we first eliminate the part of the flame CH*/OH* distribution graph that is less than 10% of the maximum CH*/OH* intensity, and take 10% of the maximum CH*/OH* intensity as the flame profile, and then find out the highest and lowest positions of the remaining part, and the distance between the two is the actual flame length sought. The CH*/OH* intensity in the flame CH*/OH* distribution diagram is smaller and more disturbed by background noise, when the fuel flow is

https://doi.org/10.1021/acsomega.3c09073
ACS Omega 2024, 9, 14997−15014

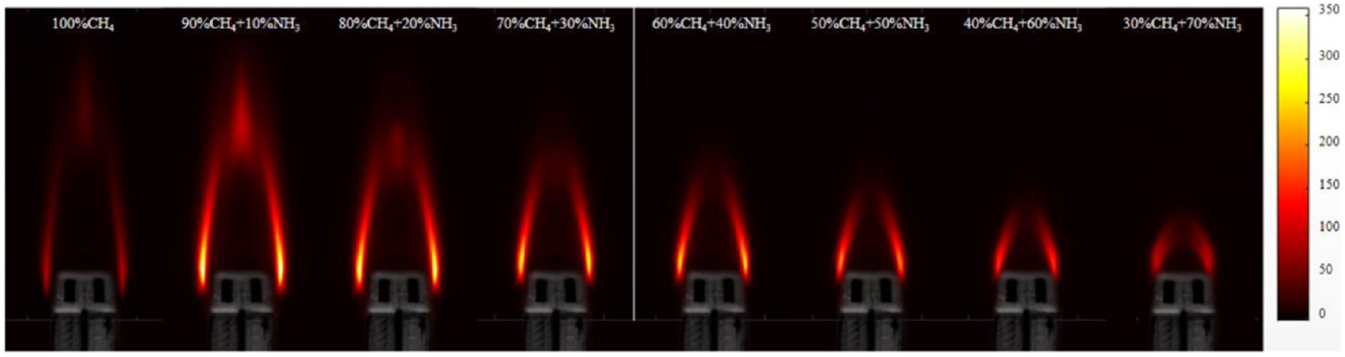

Figure 5. Pictures of CH* distribution of different components of CH_4/NH_3 fuel at a fuel flow rate of 800 mL/min at 0 mm pitch (from left to right, the fuel composition is 100%CH_4, 90%CH_4−10%NH_3, 80%CH_4−20%NH_3, 70%CH_4−30%NH_3, 60%CH_4−40%NH_3, 50%CH_4−50%NH_3, 40%CH_4−60%NH_3, and 30%CH_4−70%NH_3).

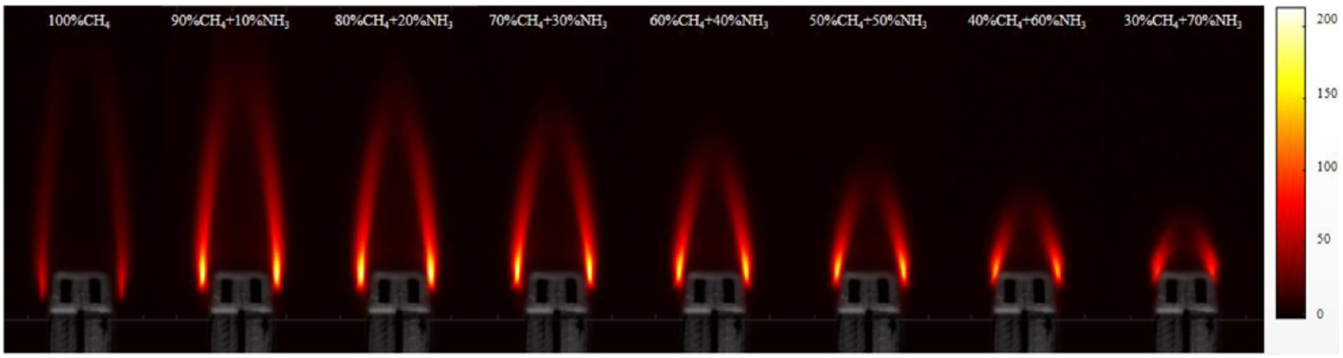

Figure 6. Pictures of OH* distribution of different components of CH_4/NH_3 fuel at a fuel flow rate of 800 mL/min at 0 mm pitch (from left to right, the fuel composition is 100%CH_4, 90%CH_4−10%NH_3, 80%CH_4−20%NH_3, 70%CH_4−30%NH_3, 60%CH_4−40%NH_3, 50%CH_4−50%NH_3, 40%CH_4−60%NH_3, and 30%CH_4−70%NH_3).

low. Therefore, the maximum CH*/OH* intensity selection range is appropriately adjusted within 15−18%, when performing low signal value rejection.

3. RESULTS AND DISCUSSION

This section investigated the double-jet flame structure with different fuel compositions and different fuel flows at different burner nozzle pitches. The flame CH* and OH* signals were taken by an ICCD camera to analyze the influence of fuel composition, fuel flow, and burner pitch on laminar flame structure from four aspects: flame appearance, CH* and OH* distribution, CH* and OH* intensity maximum, and flame size (maximum flame radius and flame length). Second, the extinction limit of the CH_4/NH_3 diffusion flame was studied to provide a stable combustion range as a quantification of the various NH_3 ratios in the mixture.

3.1. Flame Structure. This section of the experiment was divided into three parts, which were the effects of the fuel composition, fuel flow, and burner pitch on the flame structure of CH_4/NH_3 laminar flow.

3.1.1. Effect of Fuel Composition on the Structure of CH_4/NH_3 Laminar Flow Flame. The large range of CH_4/NH_3 blending ratios in the fuel makes the fuel composition one of the hot factors for flame structure research. The two diffusion flames were experimentally studied for different fuel compositions with different burner nozzle pitches. The experimental conditions in this section are shown in Table 2, and the combustion is in the laminar flow category.

3.1.1.1. Flame Appearance. The flame pictures of syngas with different compositions at a 0 mm burner pitch are given in Figure 4. The flame brightness is significantly increased when the NH_3 blending ratio is increased by only 10%. However, with the increasing proportion of NH_3 blending in the fuel composition, the flame profile of the combined flame gradually decreases.

3.1.1.2. CH and OH* Distribution.* As can be seen from Figure 5, the intensity of CH* produced during combustion is smaller, and the flame surface brightness is darker in the two diffusion flames pictures when CH_4 content in the fuel is 100%. The flame brightness is significantly increased when the NH_3 blending ratio is increased by only 10%. This suggests that 90% CH_4−10%NH_3 doping flames produce more CH* radicals than pure CH_4 combustion. However, with the increasing proportion of NH_3 blending in the fuel composition, the flame profile of the combined flame gradually decreases, the tilt angle of the flame surface decreases, and the flame develops from "slender" to "stubby".

The OH* distribution of CH_4/NH_3 flames with different blending ratios at 0 mm burner pitch at a total flow rate of 800 mL/min is given in Figure 6. It can be found that the intensity of OH* produced by the flame during combustion is small, and the flame surface brightness is dark when the blending ratio of ammonia gas is 0. The flame brightness is significantly high, indicating that the 90%CH_4−10%NH_3 blended flame produces more OH radicals than CH_4 combustion when the NH_3 blending ratio is increased by only 10%. The flame profile of the combined flame gradually decreases, the tilt angle of the flame surface decreases, and the flame develops from "slender"

https://doi.org/10.1021/acsomega.3c09073
ACS Omega 2024, 9, 14997−15014

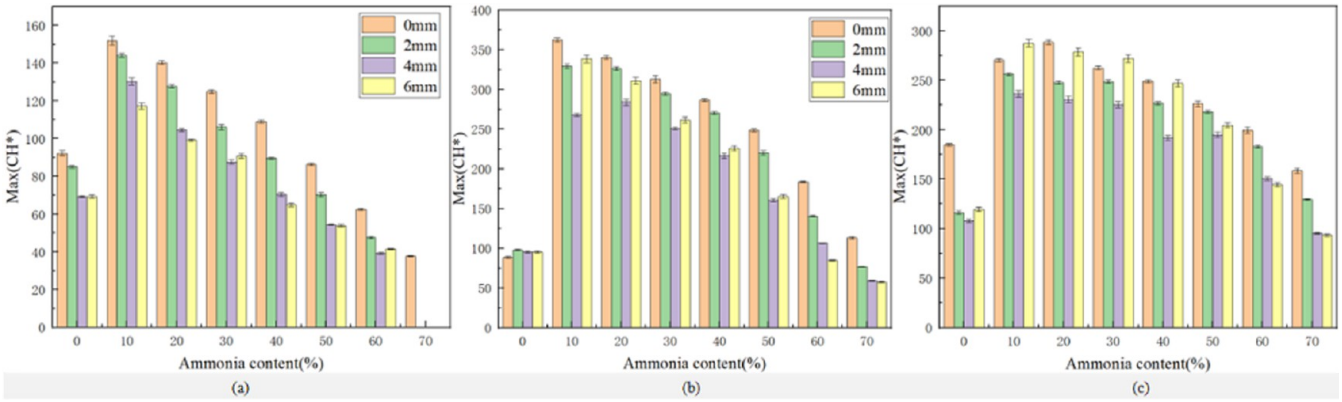

Figure 7. Maximum CH* signal intensity of CH_4/NH_3 flames at different fuel compositions and burner pitches for 3 total fuel flows ((a) 400 mL/min, (b) 600 mL/min, (c) 800 mL/min).

to "stubby" when the proportion of NH_3 blending in the fuel composition increases. Due to the low flammability of ammonia, the NO generation reaction is insensitive to OH radicals and sensitive to NH_i radicals when the ammonia blending ratio is low because the NO generation reaction is limited by the low concentration of NH_i radicals. The sensitivity of NO to OH radicals will increase with the increase of ammonia blending ratio, so the OH radical concentration will decrease with the increase of ammonia blending ratio.[40]

Comparing Figures 5 and 6, it can be seen that the CH* flame is bullet-shaped, and the OH* flame is streamlined. This is because both CH* and OH* are mainly distributed on the flame front, but the distribution of OH* is closer to the burner nozzle and CH* is more concentrated downstream of the flame. This may be due to the fact that O_2 and fuel come into contact with each other at the nozzle exit, rapidly producing large amounts of OH* and forming a flame front. OH* is still present in the fully developed section downstream of the flame,[41] but little CH* is observed.[42] At the root of the flame, OH* is distributed on the outside of the front, while CH* is distributed on the inside of the front. This is because O_2 is an important reactant in the formation reaction of OH* and the consumption reaction of CH*.[43] For low-rotation diffusion flames, O_2 is essentially absent inside the front, almost no fuel is present outside the front, and chemical reactions are essentially present on the flame front.

3.1.1.3. CH Intensity Maximum, OH* Intensity Maximum.* The CH* radical has long been considered an appropriate marker for the inner reaction zone in non-premixed and premixed hydrocarbon flames because its location marks the final step in the decomposition of hydrocarbon fuels.[37] Narrow spatial distribution of CH* radicals with flame position and exothermic rate and their disappearance has been shown to be strongly correlated with flame extinction.[37] Previous turbulent combustion studies have used CH layers obtained from planar laser-induced fluorescence (PLIF) diagnostics to visualize and study turbulence−chemistry interactions, including flame wrinkling, flame propagation, flame lift-off and stabilization, and flame response from unsteady hydrodynamics.[44] In this paper, the maximum value of the CH* signal in the CH* distribution map of each flame is extracted, and the indirect analysis of heat release rate is discussed to quantify the CH* signal intensity.

The maximum value of the CH* signal intensity (Max(CH*)) of the flame at different burner pitches for fuels of different compositions at three total flow rates is given in Figure 7. Max(CH*) in the flame rises rapidly when the fuel composition changes from pure methane to ammonia blending ratio increases to 10%. The Max(CH*) multiplier is calculated to be 1.6−1.8 times greater at a fuel flow rate of 400 mL/min, 2.77−4.12 times greater at a fuel flow rate of 600 mL/min, and 1.46−2.4 times greater at a fuel flow rate of 800 mL/min. This is mainly due to the rapid increase in the rate of CH radical production after the addition of ammonia.[40] However, the overall Max(CH*) in the flame gradually decreases as the proportion of NH_3 blending increases, and the regular curves of each burner pitch are roughly similar. This is mainly because the unstretched laminar combustion rate of the mixture decreases nonlinearly with increasing ammonia concentration and the combustion intensity decreases.[25] The curves of burner 4 and 6 mm pitch in Figure 7a are similar because the flow rate is lower at this time and the combined flame is divided into two separate flames at 4 mm pitch. At 6 mm pitch, the separate flames are exposed to more oxygen, and therefore, the Max(CH*) value is higher than at 4 mm pitch. And in Figure 7c, the Max(CH*) intensity at 6 mm pitch is higher than that at 2 mm pitch and 4 mm pitch, also because of the more adequate oxygen exposure to the independent flame. The overall Max(CH*) intensity value of the flame at 600 mL/min flow rate is higher than the Max(CH*) intensity value at 400 mL/min flow rate and 800 mL/min flow rate, which is not consistent with the derived law and is a significant finding of this section of the experiment and urgently needs to be explained by the cause.

The distribution of OH* radicals is related to the thermal random motion of atoms, and Kobayashi et al. showed that the OH* concentration value in the flame is closely related to the heat release rate, and OH* is often used as a study of heat release rate.[45] If the scale of flame thickness is very thin compared to the global scale of the flame, it is reasonable to assume that the transient flame front is sufficiently thin and that the ICCD image of OH can be used to describe the transient boundary of the flame front due to the rapid increase in OH radical concentration at the flame front of the premixed flame.[46] Therefore, in this study, in order to quantitatively analyze the OH* signal intensity, the maximum value of the OH* signal in the OH* distribution map of each flame is extracted in this paper, in order to use it for indirect analysis and discussion of the heat release rate.[47−49]

The variation of the maximum value of the flame OH* signal intensity (hereafter referred to as Max(OH*)) for different compositions of CH_4/NH_3 blended fuels at different burner pitches is given in Figure 8. The intensity of OH* increases

https://doi.org/10.1021/acsomega.3c09073
ACS Omega 2024, 9, 14997−15014

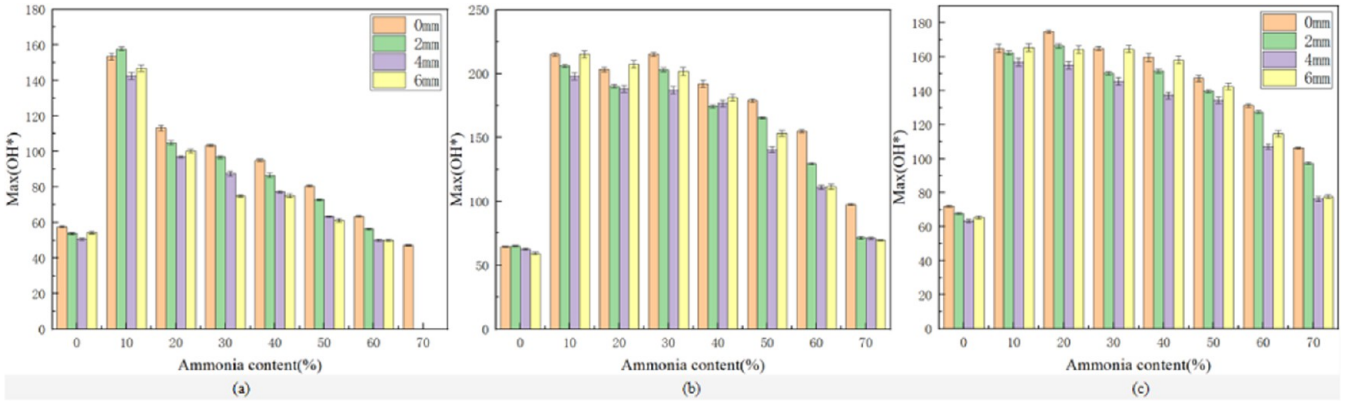

Figure 8. Maximum OH* signal intensity of CH_4/NH_3 flames at different fuel compositions and burner pitches for 3 total fuel flows ((a) 400 mL/min, (b) 600 mL/min, (c) 800 mL/min).

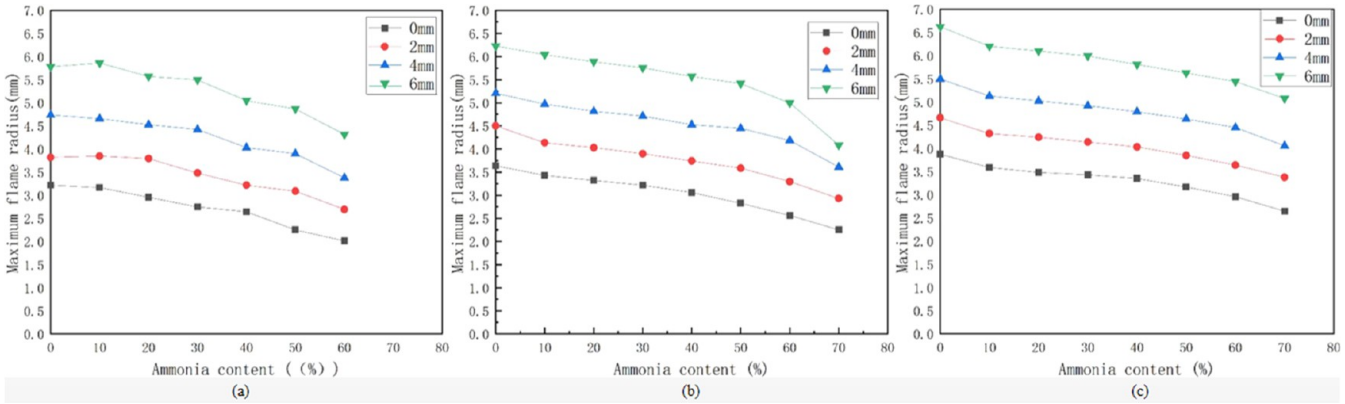

Figure 9. CH* maximum flame radius of CH_4/NH_3 flames at different fuel compositions and burner pitches for 3 total fuel flows ((a) 400 mL/min, (b) 600 mL/min, (c) 800 mL/min).

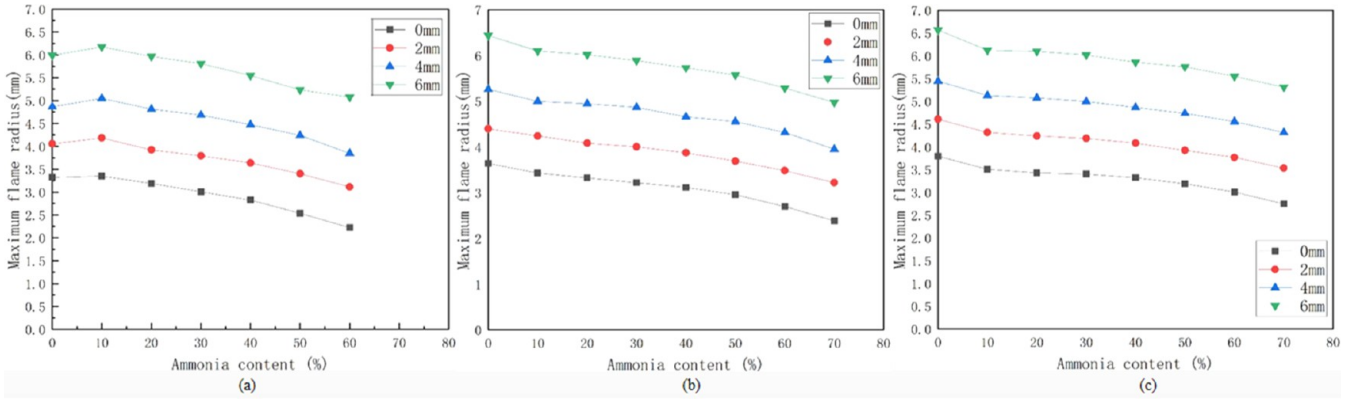

Figure 10. OH* maximum flame radius of CH_4/NH_3 flames at different fuel compositions and burner pitches for 3 total fuel flows ((a) 400 mL/min, (b) 600 mL/min, (c) 800 mL/min).

linearly after the addition of ammonia to the fuel. The Max(OH*) multiplier is calculated to be 2.6−2.9 times greater at a fuel flow rate of 400 mL/min, 3.15−3.63 times greater at a fuel flow rate of 600 mL/min, and 2.28−2.52 times greater at a fuel flow rate of 800 mL/min. Overall, the Max(OH*) in the flame gradually decreases as the proportion of ammonia blending increases. This is mainly because the volumetric exothermic rate of the flame gradually decreases as the proportion of ammonia blending increases.[10] According to Okafor et al., the consumption of H_2 and CO could promote the generation of OH radicals. H_2 and CO were consumed mainly through the chain growth reactions $H_2 + OH = H + H_2O$ and $CO + OH = H + CO_2$, and the production of OH radicals was promoted through the chain branching reaction $H + O_2 = OH + O$. As the proportion of ammonia blending increased, the concentration of H_2 and CO decreases, and so does the concentration of OH radicals.[50]

3.1.1.4. Flame Size (Maximum Flame Radius and Flame Length). Flame size is one of the most visual manifestations of the flame change process, an important indicator of burner safety and combustion efficiency, and an inevitable and important key point when studying flame interaction phenom-

https://doi.org/10.1021/acsomega.3c09073
ACS Omega 2024, 9, 14997−15014

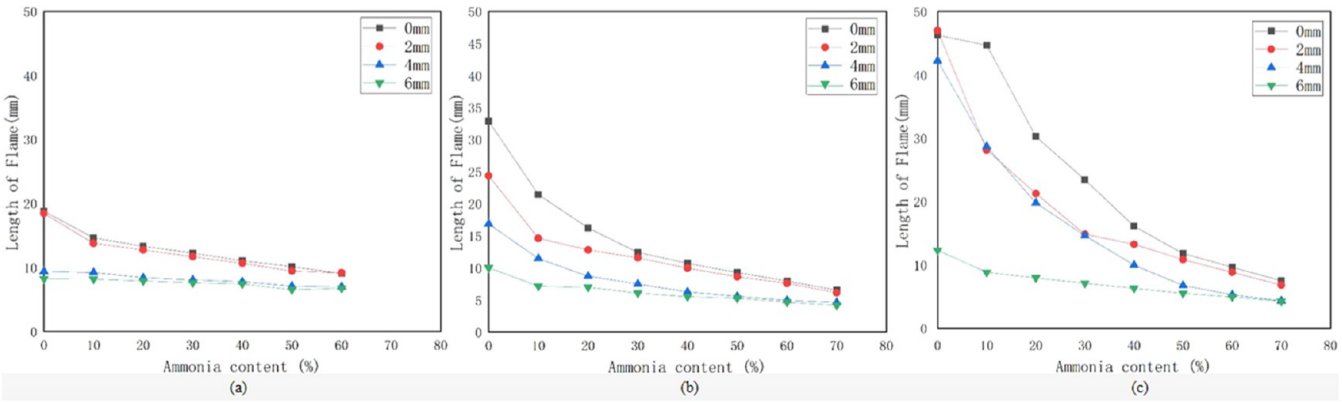

Figure 11. CH* flame lengths of CH_4/NH_3 flames at different fuel compositions and burner pitches for 3 total fuel flows ((a) 400 mL/min, (b) 600 mL/min, (c) 800 mL/min).

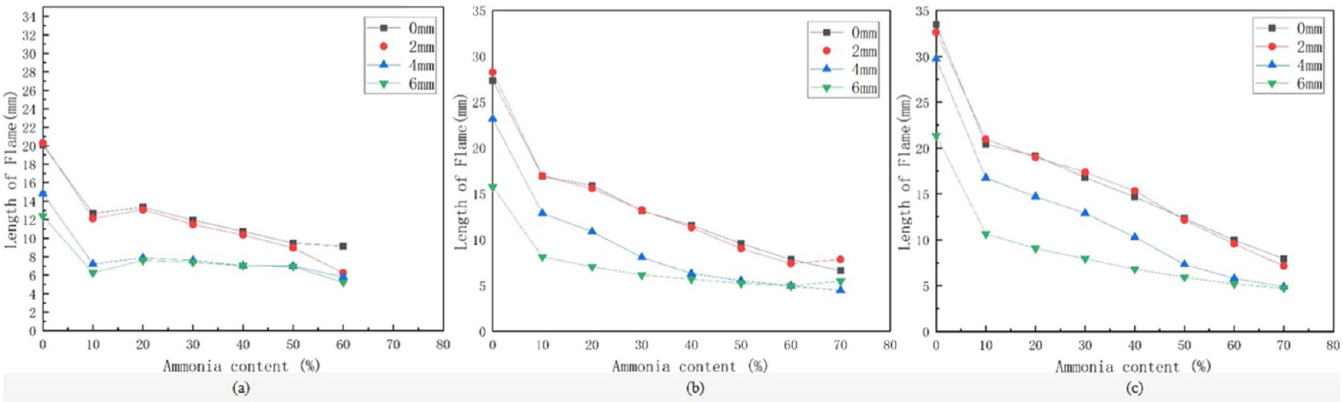

Figure 12. OH* flame lengths of CH_4/NH_3 flames at different fuel compositions and burner pitches for 3 total fuel flows ((a) 400 mL/min, (b) 600 mL/min, (c) 800 mL/min).

ena. This section compares the variation of maximum flame radius and flame length to obtain the effect law of different fuel compositions on the flame size.

The maximum flame radius of CH* for a two-jet flame burning with different CH_4/NH_3 blending ratios of fuel at 0−6 mm burner pitch is given in Figure 9. It can be seen that the maximum flame radius decreases with an increasing NH_3 content in the fuel when the burner pitch is constant, regardless of whether the flow rate increases or decreases. This is because when the NH_3 content increases, the heat diffusion rate of fuel combustion then decreases, the air diffusion capacity is relatively strong inward, the flame front then contracts inward, and the maximum flame radius decreases.[25]

The OH* maximum flame radius of the two-jet flame for different CH_4/NH_3 blending ratios of fuel combustion at 0−6 mm burner pitch is given in Figure 10, and the curve pattern is roughly similar to the above CH maximum flame radius.

The CH* flame lengths for different fuel compositions at different burner pitches for the three flow rates are given in Figure 11. It can be seen from the figure that the flame length decreases with the increase of ammonia content in the fuel. Among them, some of the fluctuations in flame length may be influenced by external ambient air curl absorption on the one hand, and may be due to experimental measurement and data processing errors on the other. The flame lengths at 4 and 6 mm spacing for NH_3 doping ratios of 0−20% are much smaller than those at 0 and 2 mm spacing in Figure 11a. This is mainly due to the smaller flow rate at this pitch, the flame front within the double-jet flame has been formed, the flame separation occurs, and almost no semimerged flame state is maintained. The flame is rapidly transformed from a semimerged flame state to an inclined separated flame state or even an independent flame state, and the flame length is sharply shortened. Flame length decreases with an increasing NH_3 content in the fuel. The increase in ammonia content decreases the overall convection time scale, and the decrease in convection time scale leads to a decrease in the distance the fuel travels before combustion, therefore shortening the flame length. In addition, free radicals, such as OH produced in the combustion process, react with the H_2 they produce, and the flame height decreases when the NH_3 content is high, while syngas with higher CH_4 content has weaker combustion stability, stronger pulsation, and large flame length.

The OH* flame lengths for different fuel compositions at different burner pitches are given in Figure 12. It can be seen from the figure that the flame length decreases with an increase in NH_3 content. The flame lengths at 4 and 6 mm pitches are smaller than those at 0 and 2 mm burner pitches. This is mainly due to the fact that at this pitch, flame fronts begin to form within the double-jet flame, and flame separation begins to occur, maintaining a smaller range of burner pitch in the semimerged flame state, and the flame is rapidly transformed from a merged flame state to an inclined separated flame state or even an independent flame state, and the flame length is drastically shortened. The top of the flame starts to produce a partial extinction, which is an important reason for the rapid decrease in

https://doi.org/10.1021/acsomega.3c09073
ACS Omega 2024, 9, 14997−15014

Figure 13. Flame appearance at 0 mm pitch for 50%CH_4−50%NH_3 fuel at different flow rates (from left to right total flow rate in the order of 400, 500, 600, 700, 800 mL/min).

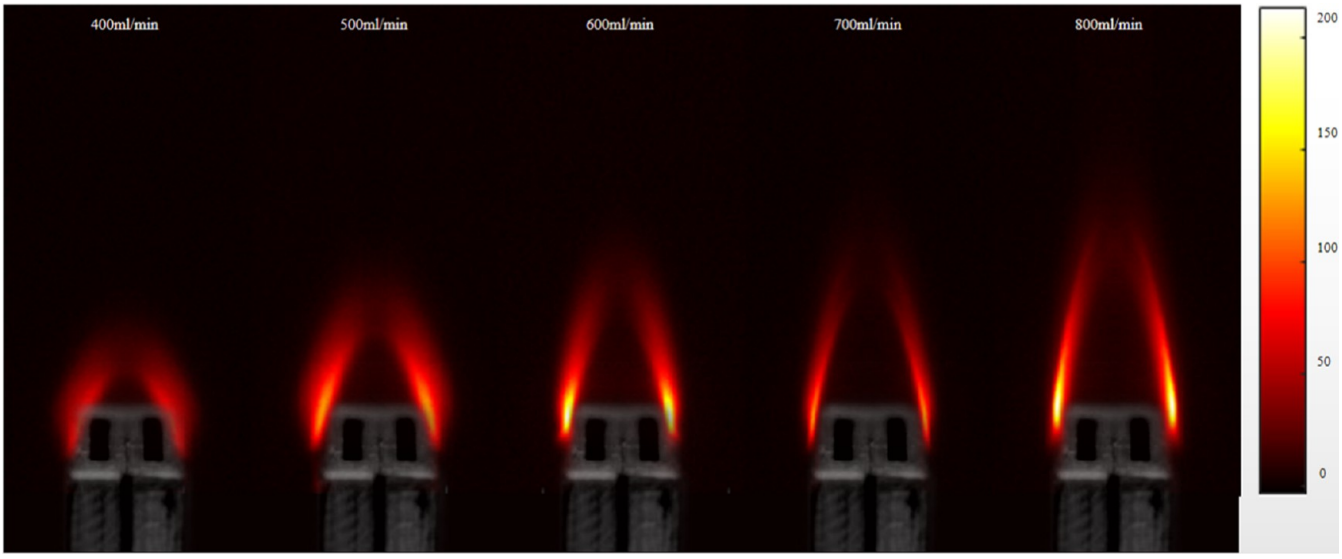

Figure 14. Distribution of CH* at 0 mm pitch for 50%CH_4−50%NH_3 fuel at different flow rates (from left to right total flow rate in the order of 400, 500, 600, 700, 800 mL/min).

flame length at this pitch, when a gap is created between the two burners.

3.1.2. Effect of Fuel Flow Rate on the Flame Structure of CH_4/NH_3 Laminar Flow. Different fields have different requirements for combustion efficiency, flame stability, and pollutant emissions, and the operating parameters of multinozzle burners are therefore complex and variable in practical application. In this section, we experimentally study the structure of the double-jet flame with different fuel flow rates. By varying the total fuel flow rate, we analyze the influence law of fuel flow rate on flame interaction in the same four aspects: flame appearance, CH* and OH* distribution, Max(CH*) and Max(OH*), and flame size, to obtain a macroscopic understanding of flame combustion characteristics and provide some basic data for future academic research and engineering applications. The experimental working conditions are shown in Table 2, and the Reynolds number range is 79−170.

3.1.2.1. Flame Appearance. The flame lengths for 50% CH_4−50%NH_3 fuel at different volume flow rates are given in Figure 13. The flame length increases with increasing fuel flow rate, which is mainly due to the fact that the total reaction time required for complete combustion becomes longer for a higher fuel flow rate and shorter residence time for a higher exit velocity, and the fuel requires a longer space to burn out.

3.1.2.2. CH and OH* Distribution.* The CH* distribution of 50%CH_4−50%NH_3 fuel at different flow rates at 0 mm pitch is

https://doi.org/10.1021/acsomega.3c09073
ACS Omega 2024, 9, 14997−15014

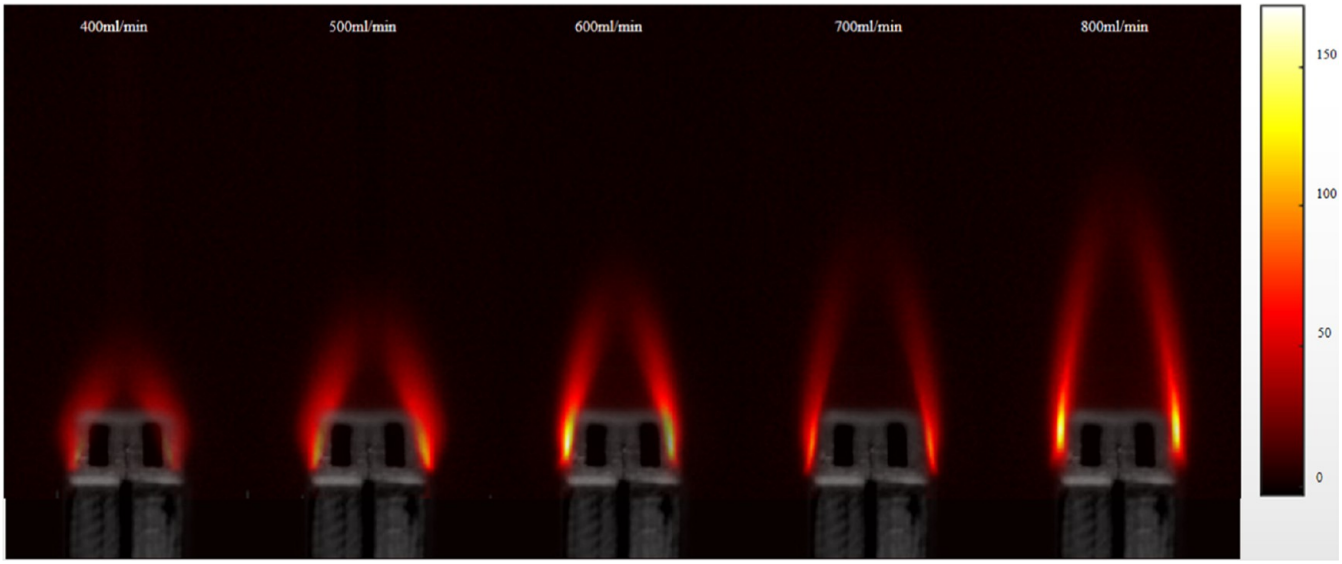

Figure 15. Distribution of OH* at 0 mm pitch for 50%CH_4−50%NH_3 fuel at different flow rates (from left to right total flow rate in the order of 400, 500, 600, 700, 800 mL/min).

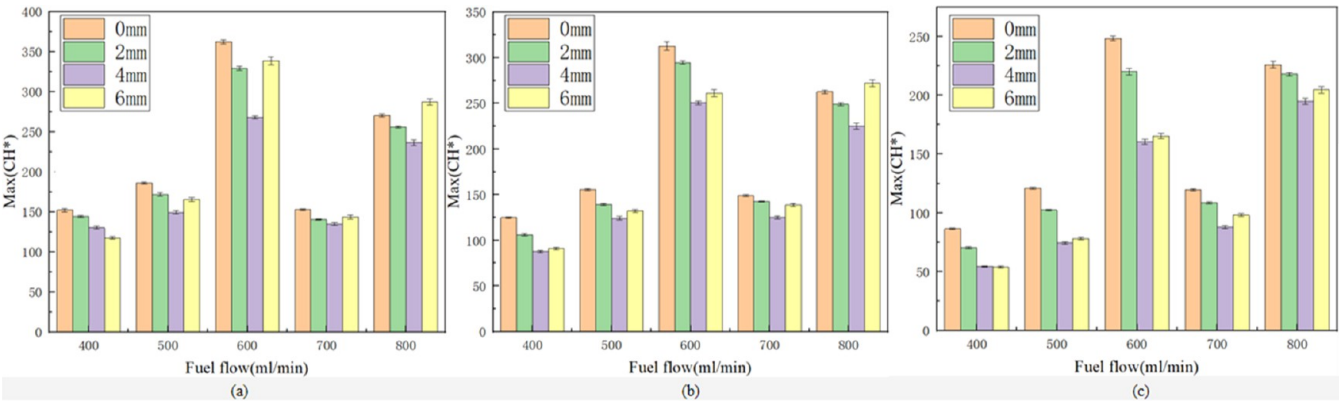

Figure 16. Max(CH*) for different fuel flow rates at 0−6 mm pitch for 3 fuel compositions ((a) 90%CH_4−10%NH_3, (b) 70%CH_4−30%NH_3, (c) 50%CH_4−50%NH_3).

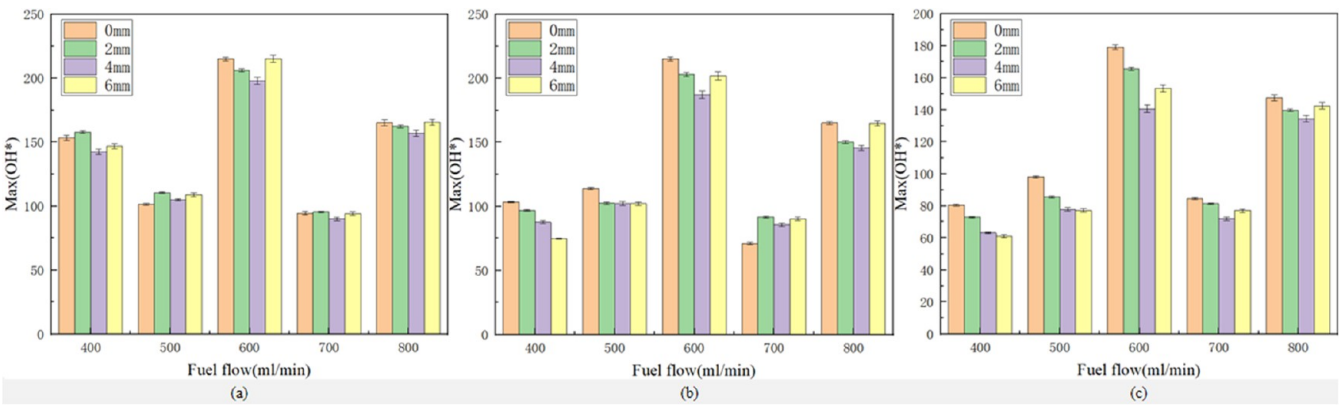

Figure 17. Max(OH*) for different fuel flow rates at 0−6 mm pitch for 3 fuel compositions ((a) 90%CH_4−10%NH_3, (b) 70%CH_4−30%NH_3, (c) 50%CH_4−50%NH_3).

given in Figure 14. It can be seen from the figure that as the fuel flow rate increases, the flame height increases, the inclination of the left and right flame fronts gradually increases, the triangular area between them lengthens, and the width of the combined flames increases. As can be seen from the figure, when the fuel flow rate increases from 400 to 600 and from 700 to 800 mL/min, the flame brightness keeps getting brighter, which means that the CH* intensity keeps increasing, which is consistent with the pattern that has been found. However, the brightness of the flame picture became darker when the flow rate increased from 600 to 700 mL/min, implying that the intensity of CH* weakened at this stage, which is contrary to the pattern found,

https://doi.org/10.1021/acsomega.3c09073
ACS Omega 2024, 9, 14997−15014

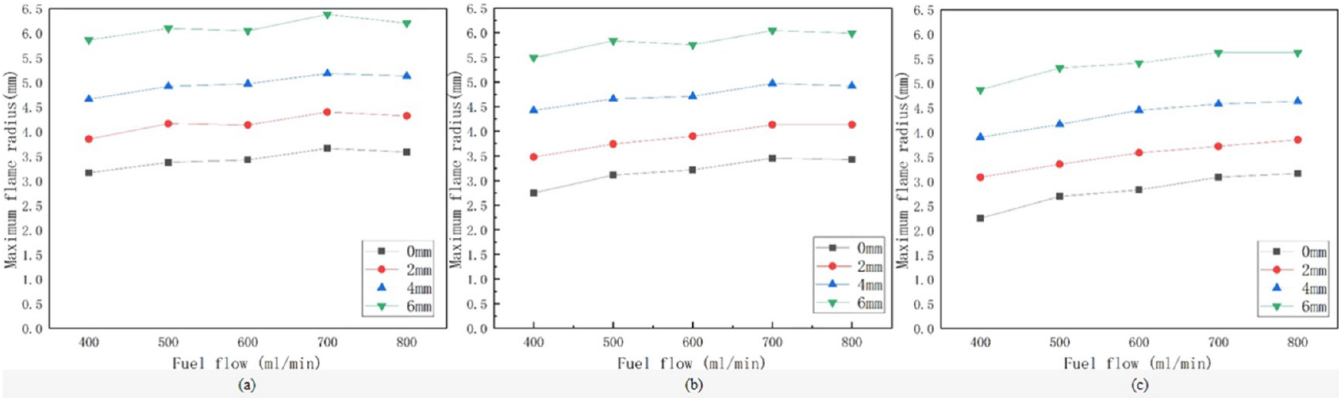

Figure 18. CH* maximum flame radius for different fuel flow rates at 0−6 mm pitch for 3 fuel compositions ((a) 90%CH_4−10%NH_3, (b) 70%CH_4−30%NH_3, (c) 50%CH_4−50%NH_3).

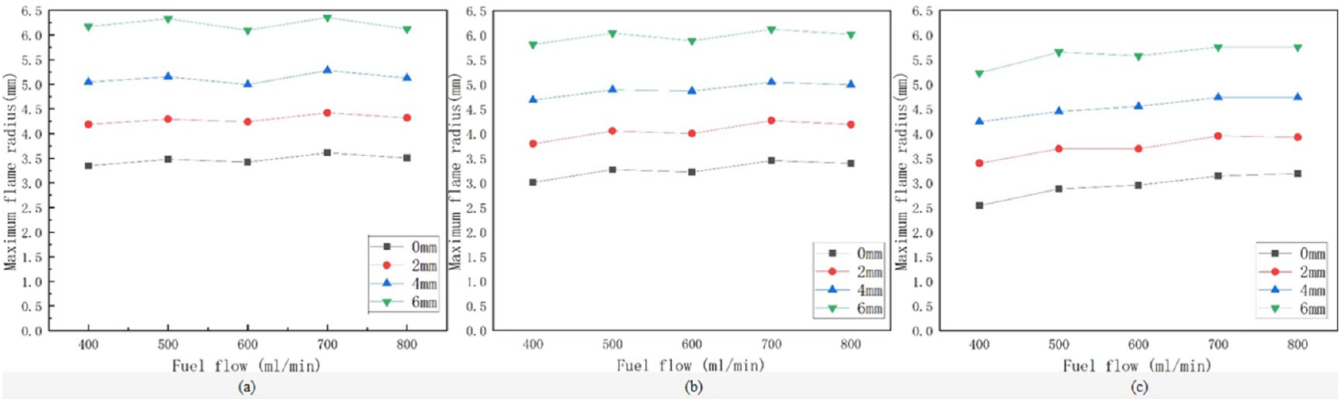

Figure 19. OH* maximum flame radius for different fuel flow rates at 0−6 mm pitch for 3 fuel compositions ((a) 90%CH_4−10%NH_3, (b) 70%CH_4−30%NH_3, (c) 50%CH_4−50%NH_3).

which may be caused by the air environment and experimental errors, and the specific reasons are not yet clear to be solved.

The OH* distribution of 50%CH_4−50%NH_3 fuel at different flow rates at 0 mm pitch is given in Figure 15. It can be seen that as the fuel flow rate increases, the flame height increases, the inclination of the left and right flame fronts gradually increases, and the width of the combined flame increases. OH* intensity gradually increases when the flow rate keeps increasing. However, the OH* intensity suddenly decreases when the fuel flow rate increases from 600 to 700 mL/min, which is contrary to the pattern that has been found, and the exact reason is not clear. But this anomalous performance is consistent with the measured CH* pattern.

3.1.2.3. CH Intensity Maximum, OH* Intensity Maximum.* Figure 16 shows the Max(CH*) in the flame for three different composition fuels at different burner pitches at flow rates of 400−800 mL/min. When the fuel flow rate increased from 400 to 600 mL/min, Max(CH*) increased, but when the fuel flow rate increased from 600 to 700 mL/min, Max(CH*) suddenly decreased, and when the fuel flow rate continued to increase to 800 mL/min, Max(CH*) gradually increased again.

Figure 17 shows the distribution of the maximum value of OH* signal intensity (hereinafter referred to as Max(OH*)) in the flame for three different compositions of fuels at different burner pitches at flow rates from 400 to 800 mL/min, and the curves are in approximate agreement with the measured CH* pattern. The difference is that the OH* intensity of the flame at a flow rate of 400 mL/min in Figure 17a is greater than that of the flame at a flow rate of 500 mL/min. This may be due to the fact that the proportion of ammonia blending has a greater effect on the flame combustion when the total flow rate is smaller or it may be due to environmental factors or experimental errors.

As is known from Figures 16 and 17, the obtained Max(CH*) and Max(OH*) curve patterns are nearly identical for the same fuel working conditions and experimental conditions. This indicates that the increase in fuel flow rate from 600 mL/min to 700 mL/min causes a rapid decrease in Max(CH*) and Max(OH*) for reasons that are not yet known.

3.1.2.4. Flame Size (Maximum Flame Radius and Flame Length). To quantitatively show the variation of the flame width, the maximum flame radius of CH* for the three compositions of fuel at different flow rates is given in Figure 18. The maximum flame radius of the double-jet flame increases with increasing fuel flow, which is also related to the need for a larger combustion pitch due to the increased amount of fuel. The maximum flame radius increased most rapidly with the increase of fuel flow rate at 0 mm pitch, especially when the fuel composition was 50%CH_4−50%NH_3, the maximum flame radius was enlarged by 1.15−1.26 times when the flow rate was increased from 400 to 800 mL/min.

The maximum flame radius of OH* for three different compositions of fuel at different flow rates is given in Figure 19, in order to discuss quantitatively the variation of the flame width. The maximum flame radius of the double-jet flame increases with increasing fuel flow but at a slower pace, which is also related to the need for a larger combustion pitch due to the

https://doi.org/10.1021/acsomega.3c09073
ACS Omega 2024, 9, 14997−15014

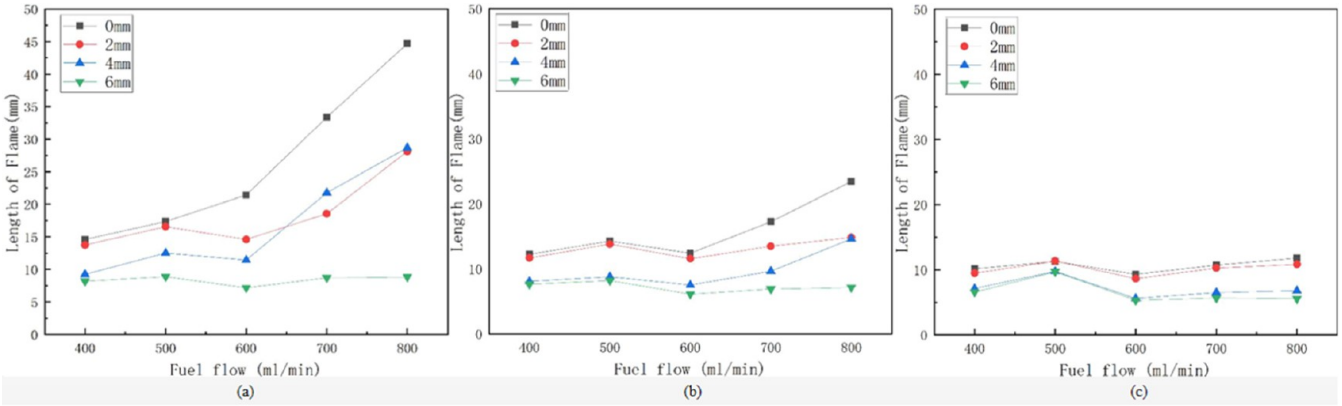

Figure 20. CH* flame length for different fuel flow rates at 0−6 mm pitch for 3 fuel compositions ((a) 90%CH_4−10%NH_3, (b)70%CH_4−30%NH_3, (c)50%CH_4−50%NH_3).

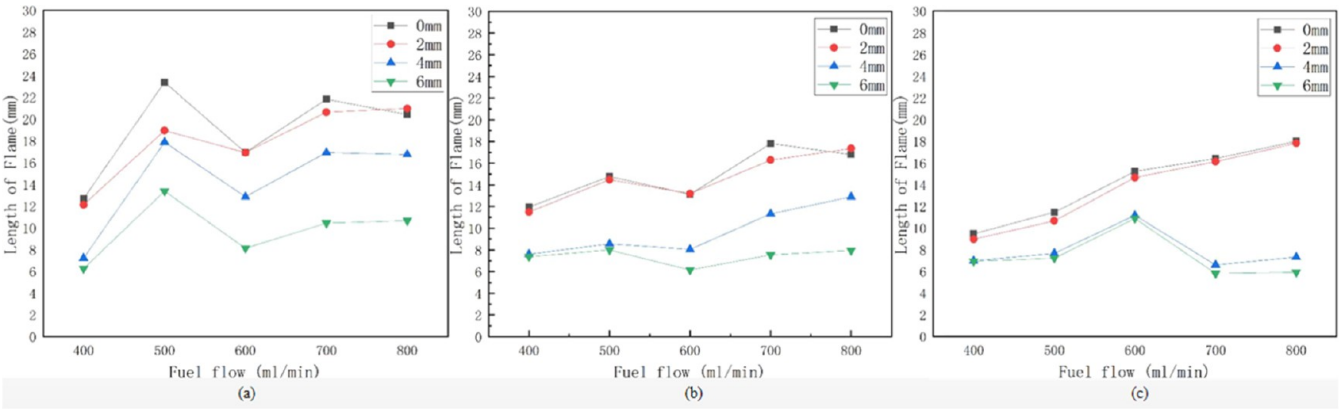

Figure 21. OH* flame length for different fuel flow rates at 0−6 mm pitch for 3 fuel compositions ((a) 90%CH_4−10%NH_3, (b) 70%CH_4−30%NH_3, (c) 50%CH_4−50%NH_3).

Figure 22. Flame appearance for a total flow rate of 800 mL/min and a blending ratio of 50%CH_4−50%NH_3 fuel burning at different pitches (from left to right burner pitch is 6, 4, 2, 0 mm).

https://doi.org/10.1021/acsomega.3c09073
ACS Omega 2024, 9, 14997−15014

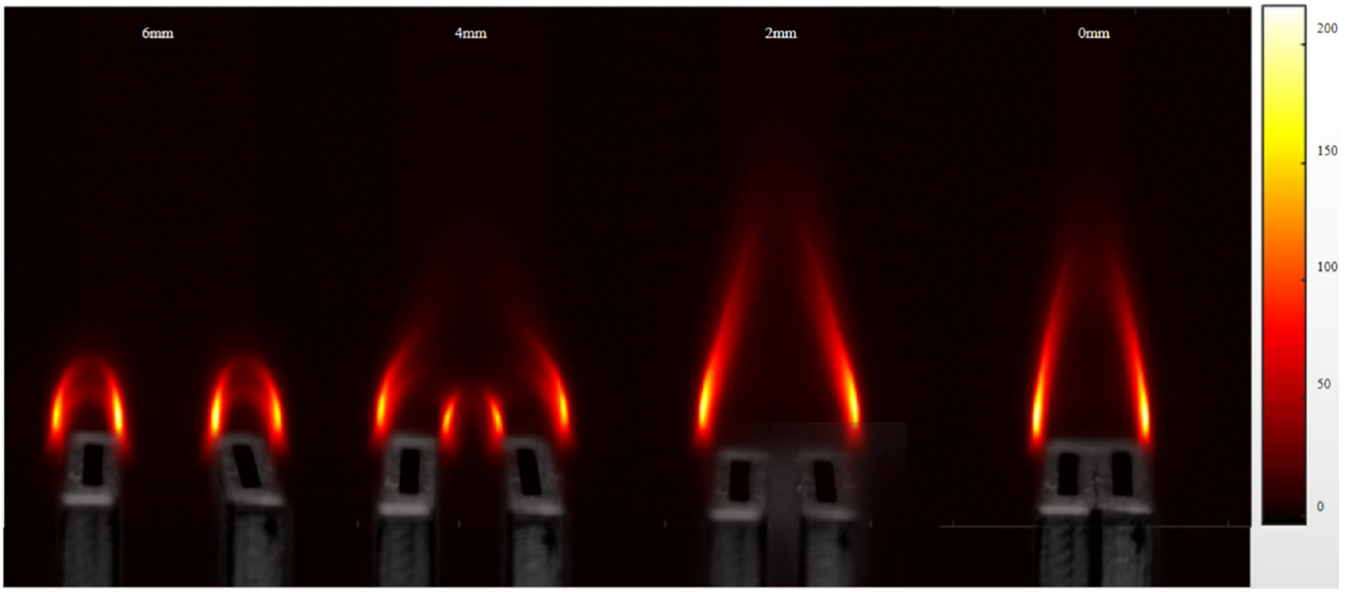

Figure 23. CH* distribution for a total flow rate of 800 mL/min and a blending ratio of 50%CH_4−50% NH_3 fuel burning at different pitches (from left to right burner pitch is 6, 4, 2, 0 mm).

increased fuel volume. The slope of the increase of the maximum flame radius with the increase of the fuel flow is greater when the ammonia content in the fuel increases, especially the maximum flame radius increases by a factor of 1.05−1.17 when the fuel composition is 50%CH_4−50%NH_3. This is also consistent with the CH* maximum flame radius curve pattern measured above.

The CH* flame lengths for three different compositions of fuel at different volume flow rates are listed in Figure 20. The flame length of a double-jet flame increases with increasing fuel flow, and such variation is nearly linear during the interdependent phase of the flame, except for the curve of individual flows. This is mainly due to the increased fuel flow rate and longer total reaction time required for complete combustion, while the exit velocity increases, the residence time becomes shorter, and the fuel requires a longer space to burn out. The change in flame length caused by the change in flow is amplified when the flames merge. As shown in Figure 20a, the flame length at 800 mL/min flow rate is 3.06 times larger than that at 400 mL/min flow rate at 0 to 2 mm pitch, while the flame length is only 1.7 times larger at 6 mm pitch. On the one hand, it may be because the two fuel flows disturb each other strongly, and the higher the fuel flow rate the more violent this disturbance, which accelerates the flow rate of fuel, the flame length further increases, when the burner pitch is very small. On the other hand, it may be that when the two jet flames are combined, the two fuels are superimposed on each other and the flow rate of the combined flames is much greater than the flow rate of the individual flames when they are separated. Thus, flame merging amplifies the trend of flame length variation.

Figure 21 shows the OH* flame lengths for three different compositions of fuel taken at different volume flow rates. As can be seen from the figure, the flame length of the double-jet flame increases with the increase of fuel flow, and the curve pattern of the flame independent of each other stage (4 mm pitch and 6 mm pitch) is about the same, and the curve pattern of the flame merging stage (0 mm pitch and 2 mm pitch) is about the same. This is mainly due to the increased fuel flow rate and longer total reaction time required for complete combustion, while the exit velocity increases, the residence time becomes shorter and the fuel requires a longer space to burn out. The flame length variation caused by the flow rate change is amplified when the flames are combined, as shown in Figure 21b for the 0−2 mm pitch, and the flame length is amplified by a factor of 1.97 at 800 mL/min flow rate compared to 400 mL/min flow rate. This is also similar to the flame length curve pattern generated by the above CH*.

3.1.3. Effect of Burner Pitch on the Structure of CH_4/NH_3 Laminar Flow Flame. 3.1.3.1. Flame Appearance. Figure 22 gives a picture of the flames of 50%CH_4−50%NH_3 fuel burned at different pitches at a flow rate of 800 mL/min. When the burner pitch is 6 mm, the two flames are independent separated flames. When the burner pitch is reduced from 6 to 4 mm, the flame transforms into a tilted separated flame and the flame height increases further; when the burner pitch is reduced to 2 mm, the flame transforms into a semicombined flame and the flame height reaches the maximum; and finally, when the burner pitch is reduced to 0 mm, the flame state is a combined flame but the flame height is lower than that of the semicombined flame.

3.1.3.2. CH and OH* Distribution.* The double-jet flame shows four states of fully independent flame, tilted separated flame, semicombined flame, and fully combined flame in turn, when the burner pitch increased, as shown in Figure 23. This change process is consistent with the flame incorporation behavior of hydrocarbon fuels studied by Hirasawa et al.[51] In this paper, it was found that for a fuel composition of 50%CH_4−50% NH_3, the two flames completely are two separate flames when the burner pitch is 6 mm. The two separated flames are tilted inward and are in a tilted separation state when the burner pitch decreases to 4 mm. The fuel diffuses downward through the gap between the burners and comes into contact with the air, and an internal flame front begins to develop between the two burner nozzles when the burner pitch decreases to 2 mm. The temperature on the fuel side is significantly elevated, leading to a diminished impact of buoyancy. However, due to the flow of fuel and the influence of diffusion, the inner flame front remains affixed to the burner nozzle below. This proximity results in an increased contact area between the fuel and air, which subsequently enhances the influence of buoyancy. Conse-

https://doi.org/10.1021/acsomega.3c09073
ACS Omega 2024, 9, 14997−15014

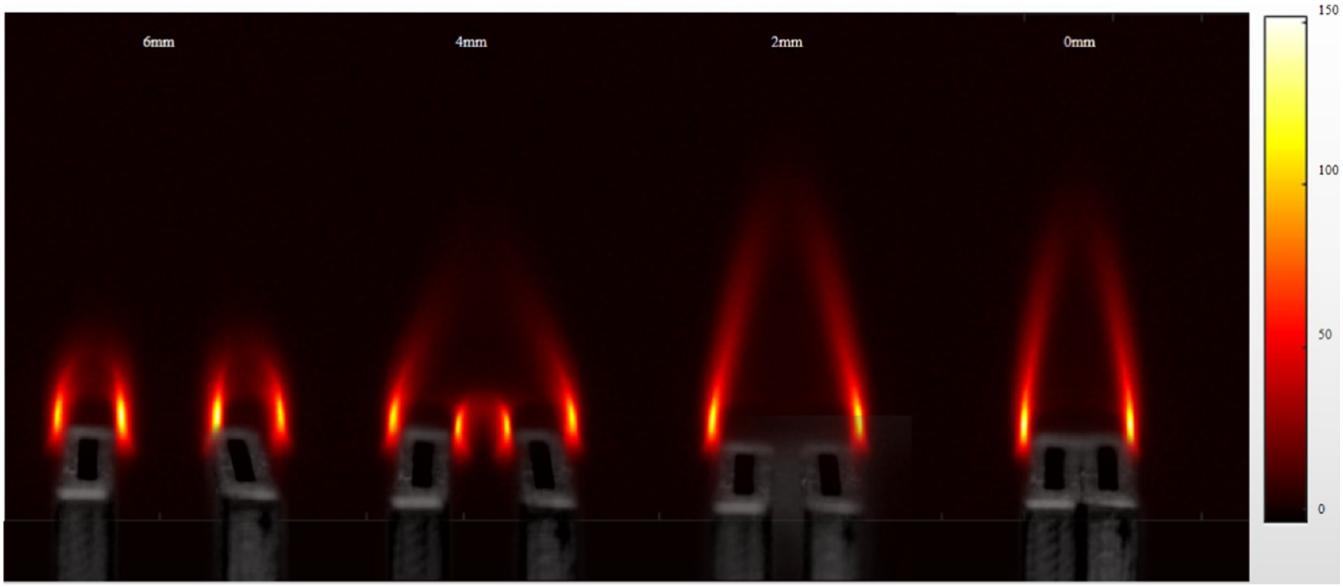

Figure 24. OH* distribution for a total flow rate of 800 mL/min and a blending ratio of 50%CH_4−50%NH_3 fuel burning at different pitches (from left to right burner pitch is 6, 4, 2, 0 mm).

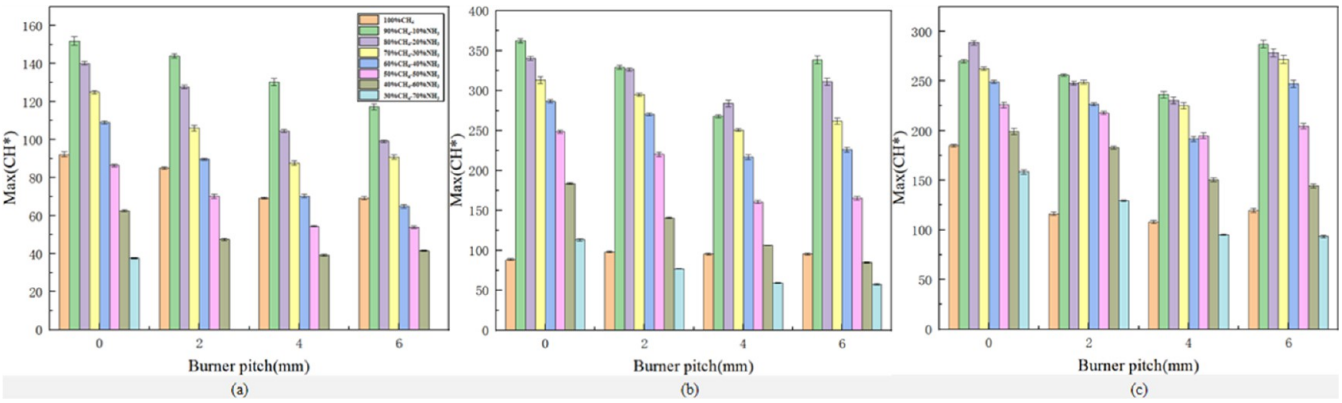

Figure 25. Max(CH*) for different fuel compositions at different burner pitches for 3 total fuel flows ((a) 400 mL/min, (b) 600 mL/min, (c) 800 mL/min).

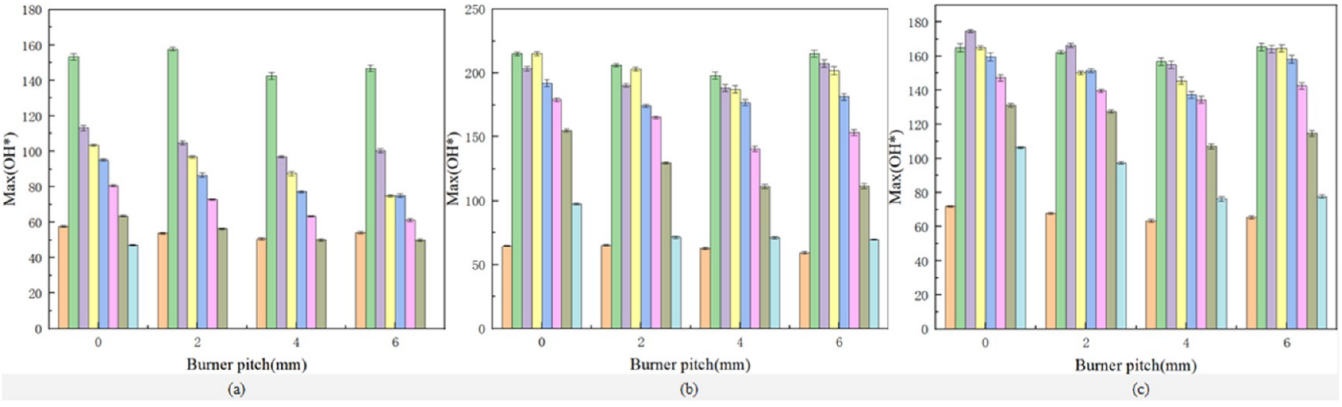

Figure 26. Max(OH*) for different fuel compositions at different burner pitches for 3 total fuel flows ((a) 400 mL/min, (b) 600 mL/min, (c) 800 mL/min).

quently, the inner flame front evolves and expands, continuously ascending upward. As the burner pitch decreases, the flame transitions from a semi-merged state to a fully merged state. It is worth noting that when the flames are combined, the flames are much higher than the corresponding separate flames.

Figure 24 shows the OH* distribution at different spacings for a total flow rate of 800 mL/min and a blending ratio of 50% CH_4−50%NH_3 fuel. As can be seen from Figure 24, with the decrease of burner pitch, the double-jet flame shows four states of completely independent flame, tilted separation flame,

https://doi.org/10.1021/acsomega.3c09073
ACS Omega 2024, 9, 14997−15014

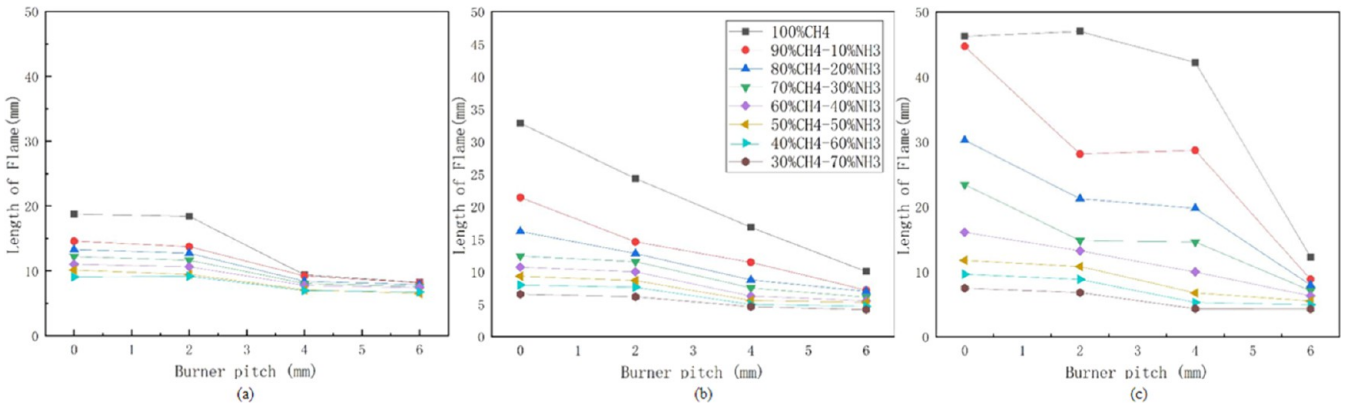

Figure 27. CH* flame length for different fuel compositions at different burner pitches for 3 total fuel flows ((a) 400 mL/min, (b) 600 mL/min, (c) 800 mL/min).

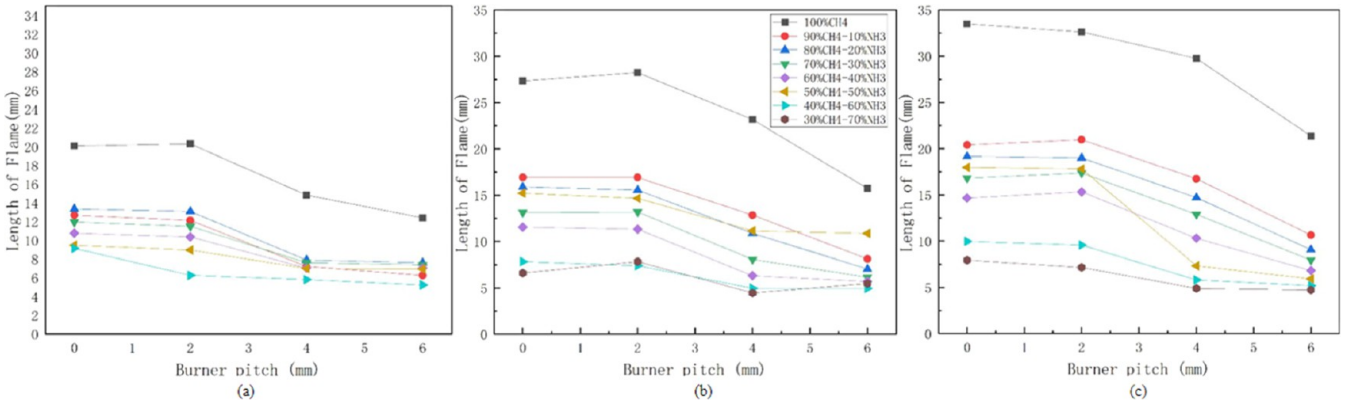

Figure 28. OH* flame length for different fuel compositions at different burner pitches for 3 total fuel flows ((a) 400 mL/min, (b) 600 mL/min, (c) 800 mL/min).

semicombined flame, and completely combined flame in turn, and this law is consistent with the above CH* distribution picture. Worth and Dawson et al. showed that the OH* autofluorescence signal in the methane double-turbulent flame interference region was enhanced with decreasing nozzle pitch.[52] This is consistent with the pattern of this experiment.

3.1.3.3. CH Intensity Maximum, OH* Intensity Maximum.* Max(CH*) in the flame gradually decreases when the burner pitch increases, as can be seen in Figure 25. This is mainly because as the burner pitch increases, the flame height decreases and the depth of flame attachment to the burner nozzle decreases, thus increasing the heat loss of the burner.[53] The local minimum at the 4 mm pitch observed in Figure 25 can be explained by the heat loss of the burner with local extinction. At 4 mm pitch, the flames are tilted apart and the inner and outer flames are formed separately; the inner flame is closer to the burner than the outer flame and is significantly affected by the burner heat loss, as shown in Figures 23 and 24. On this point, the corresponding proof has been given in the comparison of glass burners with copper burners by Kuwana et al.[54] In addition, the tip of the external flame may be partially extinguished due to the oxygen blocking effect of the internal flame, which further reduces the total heat release rate. The Max(CH*) signal from fuel combustion has a large lift, even higher than the intensity at the combined flame when the burner pitch is 4−6 mm. This may be related to the more adequate amount of oxygen when the flames are independent of each other.

As can be seen from Figure 26, Max(OH*) in the flame gradually decreases when the burner pitch increases, which is mainly because the flame height decreases as the burner pitch increases and the depth of flame attachment to the burner nozzle decreases, thus increasing the heat loss of the burner. As in the case of Max(CH*), the local minimum at the 4 mm pitch can be explained by the heat loss of the burner with local extinction.

3.1.3.4. Flame Size (Flame Length). The flame lengths produced by CH* for different compositions of fuel taken at different burner pitches for three total fuel flows are given in Figure 27. As can be seen in Figure 27, the flame length decreases with an increasing burner pitch. Some of the fluctuations in flame length may be influenced by external ambient air coiling on the one hand, and may be due to experimental measurement and data processing errors on the other. As shown in Figure 27a, the flame length decreases rapidly at 2 to 4 mm pitch, especially the smaller the ammonia blending amount in the fuel, the more obvious the flame length decrease. This is mainly due to the fact that at this pitch, flame fronts begin to form within the double-jet flame, and flame separation begins to occur, maintaining a smaller range of burner pitch in the semimerged flame state, and the flame is rapidly transformed from a merged flame state to an inclined separated flame state or even an independent flame state, and the flame length is drastically shortened. The top of the flame starts to produce partial extinction when a gap is created between the two burners, which is an important reason for the rapid decrease in flame length at this pitch. The flame length is basically constant and

https://doi.org/10.1021/acsomega.3c09073
ACS Omega 2024, 9, 14997−15014

the interaction between the two flames is small or even disappears when the burner pitch exceeds 4 mm.

Figure 28 shows the flame lengths produced by the OH* signals taken at different burner pitches for fuels of different compositions. Unlike the CH* flame length, the OH* flame length decreases somewhat more slowly as the burner pitch increases, as shown in Figure 28b. In particular, the OH* flame length hardly changes significantly with the increase of burner pitch when the ammonia blending ratio exceeds 60%. This indicates that the change in burner pitch has a greater effect on the CH* flame length than on the OH* flame length.

Since the experiments in this section manually change the burner pitch, it is meaningless to study the change of maximum flame radius with burner pitch, so only the change of flame length with burner pitch is studied in this section of flame size. In the fuel composition of 30%CH_4−70%NH_3, the flame burns only at 0 mm pitch at 400 mL/min flow rate, and the flame is extinguished under other conditions, so the curve study related to the fuel composition of 30%CH_4−70%NH_3 will be missing in the above figure.

3.2. Extinction Limit. The extinction limit is an important indicator of the combustion characteristics of combustible gases and is also extremely important for the study of CH_4/NH_3 fuel blending. The fuel needs to be able to catch fire and burn steadily in time, while also avoiding unnecessary fire conditions, such as premature or late ignition, sudden explosion, and flameout when designing the combustion device. For this reason, it is important to know the extinction limits of fuels under different conditions. There are more studies related to the upper limit of CH_4/NH_3 combustibility in previous works; however, there is a lack of research laws on the lower limit of CH_4/NH_3 fuel combustibility, especially in the presence of multinozzle burner pitch change conditions, and there is no reliable data that can be directly applied. Therefore, this experiment applies a dual-nozzle burner with adjustable pitch to measure the lower extinction limit of the CH_4/NH_3 fuel. This helps to reveal the flame propagation mechanism of CH_4/NH_3 doping combustion under different conditions and provides a clear theoretical map and scientific explanation for the basic problems of methane doping ammonia combustion stability in the future.

This experimental burner uses a double-nozzle burner with a constant outlet cross-sectional area, and the fuel properties remain almost constant when the product is transported in the pipe. The fuel flow rate is more specific to the experimental conditions than the flow rate, so Figure 29 uses the flow rate instead of the flow rate as the basic unit of the vertical coordinate. Figure 29 illustrates the extinction limit of CH_4/NH_3 for the two-nozzle burner under different conditions. The burner pitch can have the following effects on the extinction limit of the flame: first, it affects the flame merging condition of the flame combustion, which in turn affects the heat release rate of the chemical reaction; second, it directly affects the contact area of the fuel for oxygen. The fuel flow rate increases, and the lower extinction limit of the flame moves toward the direction of increasing burner pitch when the fuel composition is certain. Increasing the fuel flow rate, the change of lower extinction limit from 0 to 4 mm pitch is most obvious when the proportion of ammonia doping is 85%. Because at this time the small flow rate of the flame has been changed from the flame merging state to two separate flames, but at this time, the large flow rate of the flame presented as a double-nozzle flame merging state. The burner pitch increased to 4 mm, the flame began to show the initial separation trend, continued to increase the spacing,

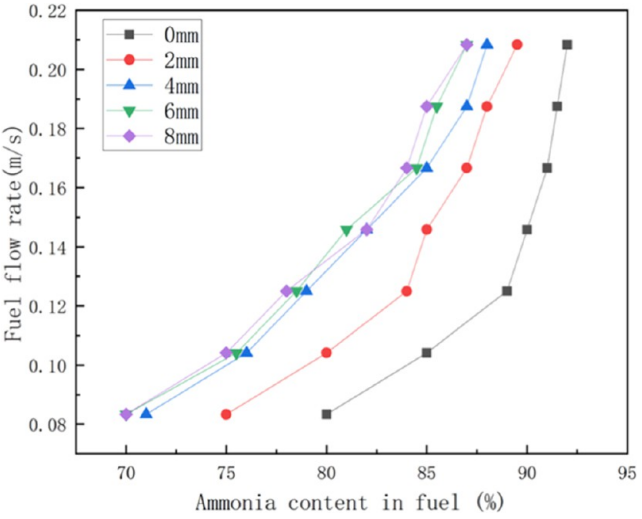

Figure 29. Extinction limit curve of methane-doped ammonia flame under different conditions of double-nozzle burner.

double nozzle combined flame gradually become two burners independent flame, and when the flame interference effect is reduced, the oxygen is more adequate, so the burner spacing factor for the change in the lower extinction limit is reduced. As the proportion of ammonia blending increases, the overall lower extinction limit changes in the direction of the burner pitch decreases when the fuel flow rate is certain, especially when the proportion of ammonia blending reaches 80% or more, if the fuel flow rate does not reach 0.1 m/s, the flame can only maintain the combustion state when the burner pitch is 0 mm. This is because the increased ammonia content reduces the laminar flame speed and raises the flame ignition point, all of which tend to extinguish the flame. The proportion of fuel blended with ammonia increases, the overall lower extinction limit moves in the direction of increasing fuel flow rate, and the slope of the curve keeps increasing when the burner pitch is certain, indicating that the fuel needs a very fast flow rate to cause flame extinction when it is rich in NH_3. The study of the lower extinction limit of CH_4/NH_3 laminar combustion in this paper provides the basic material for the future.

4. CONCLUSIONS

In this paper, we conducted an experimental study on the important scientific problem of "flame−flame interactions" in multinozzle combustion technology and discussed the flame structure and extinction limit in CH_4/NH_3 burning. CH autofluorescence signal (CH*) and OH autofluorescence signal (OH*) were studied by using an ICCD camera in variable pitch laminar diffusion flame. This paper discussed the influence of fuel composition, fuel flow, and burner pitch on flame interaction according to flame morphology, CH* intensity maximum, OH* intensity maximum, and flame size. The extinction limit of the flame was also explored by changing the experimental conditions, in order to provide some data support and research experience for the subsequent studies. The key findings from this study are summarized as follows:

(1) CH* intensity maximum and OH* intensity maximum increase rapidly when the ammonia content in the fuel grows from 0 to 10%. CH* intensity maximum and OH* intensity maximum increased 3.33−4.12 times when the fuel flow rate was 600 mL/min and ammonia content

https://doi.org/10.1021/acsomega.3c09073
ACS Omega 2024, 9, 14997−15014

increased from 0 to 10%. But the maximum values of CH* intensity and OH* intensity decrease gradually, when the ammonia content in the fuel continues to increase. The flame size decreased with increasing ammonia content in the fuel, while with increased fuel flow, the flame consolidation amplified the flame length variation trend.

(2) It was found that as the total CH_4/NH_3 fuel flow increased, the flame profile became large, the CH* intensity maximum and OH* intensity maximum increased, and the maximum flame radius and flame length increased, when the fuel composition and burner pitch were constant. However, the CH* intensity maximum and OH* intensity maximum decreased rapidly when the fuel flow increased to 700 mL/min; the reason was not clear. The flame size increased with increasing fuel flow, and flame merging amplified the flame size variation trend. The flame length amplification reached 3.06 times in the two merging diffusion flames, while in the two separated diffusion flames, the flame length amplification was only 1.7 times, when the fuel flow increased from 400 to 800 mL/min.

(3) With the increase of burner pitch, the two diffusion flames showed four states of merged flames, merging flames, inclining separated flames, and independent flames in turn. As the burner pitch increased, the CH* intensity maximum and OH* intensity maximum gradually decreased and the flame length decreased rapidly with increasing burner pitch, especially when the two diffusion flames were combined or when the amount of ammonia in the fuel composition was smaller. In this experiment, the flame length was about 1.35 to 3.5 times longer when merging than being independent.

(4) The fuel flow rate increased and the extinction limit of the flame moved in the direction of increasing burner pitch when the fuel composition was certain. The proportion of fuel blended with ammonia increased, and the extinction limit moved in the direction of decreasing burner pitch when the fuel flow rate was certain. The proportion of fuel blended with ammonia increases, and the extinction limit moved in the direction of increasing fuel flow rate when the burner pitch was certain. Under conditions close to flame extinction, excessive stretching would occur at the flame front, which would be the beginning of extinction of the entire flame due to failure to reach the minimum ignition energy. And the increased ammonia content reduced the laminar flame speed and increased the flame ignition point, all of which tended to extinguish the flame.

AUTHOR INFORMATION

Corresponding Author

Xiaohan Ren − *Institute of Thermal Science and Technology, Shandong University, Jinan 250061, China;* orcid.org/0009-0005-3142-5436; Email: renxh@sdu.edu.cn

Authors

Fanxing Meng − *Institute of Thermal Science and Technology, Shandong University, Jinan 250061, China; Institute for Advanced Technology, Shandong University, Jinan, Shandong 250061, China*

Quanwang Chen − *Shandong Institute for Product Quality Inspection, Jinan, Shandong 250102, China*

Bingbing Zheng − *Institute of Thermal Science and Technology, Shandong University, Jinan 250061, China; Institute for Advanced Technology, Shandong University, Jinan, Shandong 250061, China*

Complete contact information is available at: https://pubs.acs.org/10.1021/acsomega.3c09073

Notes

The authors declare no competing financial interest.

ACKNOWLEDGMENTS

This paper was supported by the National Natural Science Foundation of China (grant no. 52206160).

REFERENCES

(1) Chen, J.; Fei, Y.; Wan, Z. The relationship between the development of global maritime fleets and GHG emission from shipping. *J. Environ. Manage.* **2019**, *242*, 31−39.

(2) Maggio, G.; Cacciola, G. When will oil, natural gas, and coal peak? *Fuel* **2012**, *98*, 111−123.

(3) Yang, S. J.; Jung, H.; Kim, T.; Park, C. R. Recent advances in hydrogen storage technologies based on nanoporous carbon materials. *Prog. Nat. Sci.: Mater. Int.* **2012**, *22* (6), 631−638.

(4) Lee, J. H.; Lee, S. I.; Kwon, O. C. Effects of ammonia substitution on hydrogen/air flame propagation and emissions. *Int. J. Hydrogen Energy* **2010**, *35* (20), 11332−11341.

(5) Lan, R.; Irvine, J. T. S.; Tao, S. Ammonia and related chemicals as potential indirect hydrogen storage materials. *Int. J. Hydrogen Energy* **2012**, *37* (2), 1482−1494.

(6) Kandemir, T.; Schuster, M. E.; Senyshyn, A.; Behrens, M.; Schlogl, R. The Haber-Bosch process revisited: on the real structure and stability of "ammonia iron" under working conditions. *Angew. Chem., Int. Ed.* **2013**, *52* (48), 12723−12726.

(7) Kobayashi, H.; Hayakawa, A.; Somarathne, K. D. K. A.; Okafor, E. C. Science and technology of ammonia combustion. *Proc. Combust. Inst.* **2019**, *37* (1), 109−133.

(8) Frigo, S.; Gentili, R. Analysis of the behaviour of a 4-stroke Si engine fuelled with ammonia and hydrogen. *Int. J. Hydrogen Energy* **2013**, *38* (3), 1607−1615.

(9) Valera-Medina, A.; Marsh, R.; Runyon, J.; Pugh, D.; Beasley, P.; Hughes, T.; Bowen, P. Ammonia−methane combustion in tangential swirl burners for gas turbine power generation. *Appl. Energy* **2017**, *185*, 1362−1371.

(10) Xiao, H.; Valera-Medina, A.; Bowen, P. J. Study on premixed combustion characteristics of co-firing ammonia/methane fuels. *Energy* **2017**, *140*, 125−135.

(11) Valera-Medina, A.; Pugh, D. G.; Marsh, P.; Bulat, G.; Bowen, P. Preliminary study on lean premixed combustion of ammonia-hydrogen for swirling gas turbine combustors. *Int. J. Hydrogen Energy* **2017**, *42* (38), 24495−24503.

(12) Hayakawa, A.; Goto, T.; Mimoto, R.; Arakawa, Y.; Kudo, T.; Kobayashi, H. Laminar burning velocity and Markstein length of ammonia/air premixed flames at various pressures. *Fuel* **2015**, *159*, 98−106.

(13) Murai, R.; Omori, R.; Kano, R.; Tada, Y.; Higashino, H.; Nakatsuka, N.; Hayashi, J.; Akamatsu, F.; Iino, K.; Yamamoto, Y. The radiative characteristics of NH 3 /N 2 /O 2 non-premixed flame on a 10 kW test furnace. *Energy Procedia* **2017**, *120*, 325−332.

(14) Valera-Medina, A.; Xiao, H.; Owen-Jones, M.; David, W. I. F.; Bowen, P. J. Ammonia for power. *Prog. Energy Combust. Sci.* **2018**, *69*, 63−102.

(15) Ni, S.; Zhao, D.; You, Y.; Huang, Y.; Wang, B.; Su, Y. NOx emission and energy conversion efficiency studies on ammonia-powered micro-combustor with ring-shaped ribs in fuel-rich combustion. *J. Cleaner Prod.* **2021**, *320*, No. 128901.

(16) Kan, S. Y.; Chen, B.; Wu, X. F.; Chen, Z. M.; Chen, G. Q. Natural gas overview for world economy: From primary supply to final demand via global supply chains. *Energy Policy* **2019**, *124*, 215−225.

https://doi.org/10.1021/acsomega.3c09073
ACS Omega 2024, 9, 14997−15014

(17) Ku, J. W.; Choi, S.; Kim, H. K.; Lee, S.; Kwon, O. C. Extinction limits and structure of counterflow nonpremixed methane-ammonia/air flames. *Energy* **2018**, *165*, 314−325.
(18) Ku, J. W.; Ahn, Y. J.; Kim, H. K.; Kim, Y. H.; Kwon, O. C. Propagation and emissions of premixed methane-ammonia/air flames. *Energy* **2020**, *201*, No. 117632.
(19) Ramos, C. F.; Rocha, R. C.; Oliveira, P. M. R.; Costa, M.; Bai, X.-S. Experimental and kinetic modelling investigation on NO, CO and NH3 emissions from NH3/CH4/air premixed flames. *Fuel* **2019**, *254*, No. 115693.
(20) Shu, T.; Xue, Y.; Zhou, Z.; Ren, Z. An experimental study of laminar ammonia/methane/air premixed flames using expanding spherical flames. *Fuel* **2021**, *290*, No. 120003.
(21) Colson, S.; Kuhni, M.; Hayakawa, A.; Kobayashi, H.; Galizzi, C.; Escudié, D. Stabilization mechanisms of an ammonia/methane non-premixed jet flame up to liftoff. *Combust. Flame* **2021**, *234*, No. 111657.
(22) Skreiberg, Ø.; Kilpinen, P.; Glarborg, P. Ammonia chemistry below 1400 K under fuel-rich conditions in a flow reactor. *Combust. Flame* **2004**, *136* (4), 501−518.
(23) Tian, Z.; Li, Y.; Zhang, L.; Glarborg, P.; Qi, F. An experimental and kinetic modeling study of premixed NH3/CH4/O2/Ar flames at low pressure. *Combust. Flame* **2009**, *156* (7), 1413−1426.
(24) Ji, L.; Wang, J.; Hu, G.; Mao, R.; Zhang, W.; Huang, Z. Experimental study on structure and blow-off characteristics of NH3/CH4 co-firing flames in a swirl combustor. *Fuel* **2022**, *314*, No. 123027.
(25) Xiao, H.; Lai, S.; Valera-Medina, A.; Li, J.; Liu, J.; Fu, H. Study on counterflow premixed flames using high concentration ammonia mixed with methane. *Fuel* **2020**, *275*, No. 117902.
(26) Kumar, P.; Meyer, T. R. Experimental and modeling study of chemical-kinetics mechanisms for H2−NH3−air mixtures in laminar premixed jet flames. *Fuel* **2013**, *108*, 166−176.
(27) Ichikawa, A.; Hayakawa, A.; Kitagawa, Y.; Somarathne, K.; Kudo, T.; Kobayashi, H. Laminar burning velocity and Markstein length of ammonia/hydrogen/air premixed flames at elevated pressures. *Int. J. Hydrogen Energy* **2015**, *40* (30), 9570−9578.
(28) Lee, J. H.; Kim, J. H.; Park, J. H.; Kwon, O. C. Studies on properties of laminar premixed hydrogen-added ammonia/air flames for hydrogen production. *Int. J. Hydrogen Energy* **2010**, *35* (3), 1054−1064.
(29) Lhuillier, C.; Brequigny, P.; Lamoureux, N.; Contino, F.; Mounaïm-Rousselle, C. Experimental investigation on laminar burning velocities of ammonia/hydrogen/air mixtures at elevated temperatures. *Fuel* **2020**, *263*, No. 116653.
(30) Han, X. L.; Wang, Z. H.; Costa, M.; Sun, Z. W.; He, Y.; Cen, K. F. Experimental and kinetic modeling study of laminar burning velocities of NH3/air, NH3/H2/air, NH3/CO/air and NH3/CH4/air premixed flames. *Combust. Flame* **2019**, *206*, 214−226.
(31) Okafor, E. C.; Naito, Y.; Colson, S.; Ichikawa, A.; Kudo, T.; Hayakawa, A.; Kobayashi, H. Experimental and numerical study of the laminar burning velocity of CH4−NH3−air premixed flames. *Combust. Flame* **2018**, *187*, 185−198.
(32) Han, X. L.; Wang, Z. H.; He, Y.; Zhu, Y. Q.; Cen, K. F. Experimental and kinetic modeling study of laminar burning velocities of NH3/syngas/air premixed flames. *Combust. Flame* **2020**, *213*, 1−13.
(33) Wang, S. X.; Wang, Z. H.; Elbaz, A. M.; Han, X. L.; He, Y.; Costa, M.; Konnov, A. A.; Roberts, W. L. Experimental study and kinetic analysis of the laminar burning velocity of NH3/syngas/air, NH3/CO/air and NH3/H2/air premixed flames at elevated pressures. *Combust. Flame* **2020**, *221*, 270−287.
(34) Glarborg, P.; Miller, J. A.; Ruscic, B.; Klippenstein, S. J. Modeling nitrogen chemistry in combustion. *Prog. Energy Combust. Sci.* **2018**, *67*, 31−68.
(35) Asai, T.; Dodo, S.; Karishuku, M.; Yagi, N.; Akiyama, Y.; Hayashi, A. *Performance of Multiple-Injection Dry Low-NOx Combustor on Hydrogen-Rich Syngas Fuel in an IGCC Pilot Plant*, ASME Turbo Expo: Turbine Technical Conference and Exposition; ASME, 2014.
(36) Tacina, R.; Wey, C.; Laing, P.; Mansour, A. In *Sector Tests of a Low NOx, Lean-Direct-Injection, Multipoint Integrated Module Combustor Concept*, ASME Turbo Exposition 2002: Power for Land, Sea, and Air; ASME, 2002; pp 533−544.
(37) Karnani, S.; Dunn-Rankin, D. Visualizing CH* chemiluminescence in sooting flames. *Combust. Flame* **2013**, *160* (10), 2275−2278.
(38) Marchese, A. J.; Dryer, F. L.; Nayagam, V.; Colantonio, R. O. Hydroxyl radical chemiluminescence imaging and the structure of microgravity droplet flames. *Symp. (Int.) Combust.* **1996**, *26* (1), 1219−1226.
(39) Li, J.; Huang, H. Y.; Bai, Y.; Li, S. J.; Kobayashi, N. Combustion and heat release characteristics of hydrogen/air diffusion flame on a micro jet array burner. *Int. J. Hydrogen Energy* **2018**, *43* (29), 13563−13574.
(40) Zhu, X.; Khateeb, A. A.; Roberts, W. L.; Guiberti, T. F. Chemiluminescence signature of premixed ammonia-methane-air flames. *Combust. Flame* **2021**, *231*, No. 111508.
(41) Paa, W.; Müller, D.; Stafast, H.; Triebel, W. Flame turbulences recorded at 1 kHz using planar laser induced fluorescence upon hot band excitation of OH radicals. *Appl. Phys. B* **2006**, *86* (1), 1−5.
(42) Kiefer, J.; Li, Z. S.; Zetterberg, J.; Bai, X. S.; Aldén, M. Investigation of local flame structures and statistics in partially premixed turbulent jet flames using simultaneous single-shot CH and OH planar laser-induced fluorescence imaging. *Combust. Flame* **2008**, *154* (4), 802−818.
(43) Ballester, J.; Hernández, R.; Sanz, A.; Smolarz, A.; Barroso, J.; Pina, A. Chemiluminescence monitoring in premixed flames of natural gas and its blends with hydrogen. *Proc. Combust. Inst.* **2009**, *32* (2), 2983−2991.
(44) Ueda, T.; Shimura, M.; Tanahashi, M.; Miyauchi, T. Measurement of three-dimensional flame structure by combined laser diagnostics. *J. Mech. Sci. Technol.* **2009**, *23* (7), 1813−1820.
(45) Kobayashi, H.; Seyama, K.; Hagiwara, H.; Ogami, Y. Burning velocity correlation of methane/air turbulent premixed flames at high pressure and high temperature. *Proc. Combust. Inst.* **2005**, *30* (1), 827−834.
(46) Zhang, M.; Wang, J.; Xie, Y.; Wei, Z.; Jin, W.; Huang, Z.; Kobayashi, H. Measurement on instantaneous flame front structure of turbulent premixed CH4/H2/air flames. *Exp. Therm. Fluid Sci.* **2014**, *52*, 288−296.
(47) Somarathne, K. D. K. A.; Hayakawa, A.; Kobayashi, H. Numerical investigation on the combustion characteristics of turbulent premixed ammonia/air flames stabilized by a swirl burner. *J. Fluid Sci. Technol.* **2016**, *11* (4), No. JFST0026.
(48) Somarathne, K. D. K. A.; Hatakeyama, S.; Hayakawa, A.; Kobayashi, H. Numerical study of a low emission gas turbine like combustor for turbulent ammonia/air premixed swirl flames with a secondary air injection at high pressure. *Int. J. Hydrogen Energy* **2017**, *42* (44), 27388−27399.
(49) Somarathne, K. D. K. A.; Colson, S.; Hayakawa, A.; Kobayashi, H. Modelling of ammonia/air non-premixed turbulent swirling flames in a gas turbine-like combustor at various pressures. *Combust. Theory Modell.* **2018**, *22* (5), 973−997.
(50) Okafor, E. C.; Somarathne, K. D. K. A.; Hayakawa, A.; Kudo, T.; Kurata, O.; Iki, N.; Kobayashi, H. Towards the development of an efficient low-NOx ammonia combustor for a micro gas turbine. *Proc. Combust. Inst.* **2019**, *37* (4), 4597−4606.
(51) Hirasawa, T.; Gotanda, K.; Masuda, H.; Nakamura, Y. Impact of Flame−Flame Interactions in Identical Twin Diffusion Microflames. *Combust. Sci. Technol.* **2012**, *184* (10−11), 1651−1663.
(52) Worth, N. A.; Dawson, J. R. Tomographic reconstruction of OH* chemiluminescence in two interacting turbulent flames. *Meas. Sci. Technol.* **2013**, *24* (2), No. 024013.
(53) Tyagi, A.; Boxx, I.; Peluso, S.; O'Connor, J. Statistics and topology of local flame−flame interactions in turbulent flames. *Combust. Flame* **2019**, *203*, 92−104.
(54) Kuwana, K.; Kato, S.; Kosugi, A.; Hirasawa, T.; Nakamura, Y. Experimental and theoretical study on the interaction between two identical micro-slot diffusion flames: Burner pitch effects. *Combust. Flame* **2016**, *165*, 346−353.

https://doi.org/10.1021/acsomega.3c09073
ACS Omega 2024, 9, 14997−15014